Icarus 179 (2005)

Layering stratigraphy of eastern Coprates and northern Capri Chasmata, Mars

Ross A. Beyer[1 2] and Alfred S. McEwen[3]

Department of Planetary Sciences, The University of Arizona, Tucson, AZ 85721, USA

Received 25 October 2004; revised 25 May 2005

Abstract

Distinct competent layers are observed in the slopes of eastern Coprates Chasma, part of the Valles Marineris system on Mars. Our observations indicate that the stratigraphy of Coprates Chasma consists of alternating thin strong layers and thicker sequences of relatively weak layers. The strong, competent layers maintain steeper slopes and play a major role in controlling the overall shape and geomorphology of the chasmata slopes. The topmost competent layer in this area is well preserved and easy to identify in outcrops on the northern rim of Coprates Chasma less than 100 m below the southern Ophir Planum surface. The volume of the topmost emplaced layer is at least 70 km^3 and may be greater than 2100 km^3 if the unit underlies most of Ophir Planum. The broad extent of this layer allows us to measure elevation offsets within the north rim of the chasma and in a freestanding massif within Coprates Chasma where the layer is also observed. Rim outcrop morphology and elevation differences between Ophir and Aurorae Plana may be indicative of the easternmost extent of the topmost competent layer. These observations allow an insight into the depositional processes that formed the stratigraphic stack into which this portion of the Valles Marineris is carved, and they present a picture of some of the last volcanic activity in this area. Furthermore, the elevation offsets within the layer are evidence of significant subsidence of the massif and surrounding material.

Keywords: Geological processes; Geophysics; Image processing; Mars, surface; Surfaces, planets; Tectonics; Terrestrial planets; Volcanism

Citation: Beyer, Ross A. and Alfred S. McEwen, Layering stratigraphy of eastern Coprates and northern Capri Chasmata, Mars, *Icarus*, 179, Issue 1, p. 1-23, 2005, doi:10.1016/j.icarus.2005.06.014. To view the published open abstract and find a link to the published paper, go to http://dx.doi.org and enter the DOI.

[1]Now at NASA Ames Research Center, MS 245-3, Moffett Field, CA 94035
[2]E-mail: rbeyer@arc.nasa.gov
[3]E-mail: mcewen@lpl.arizona.edu

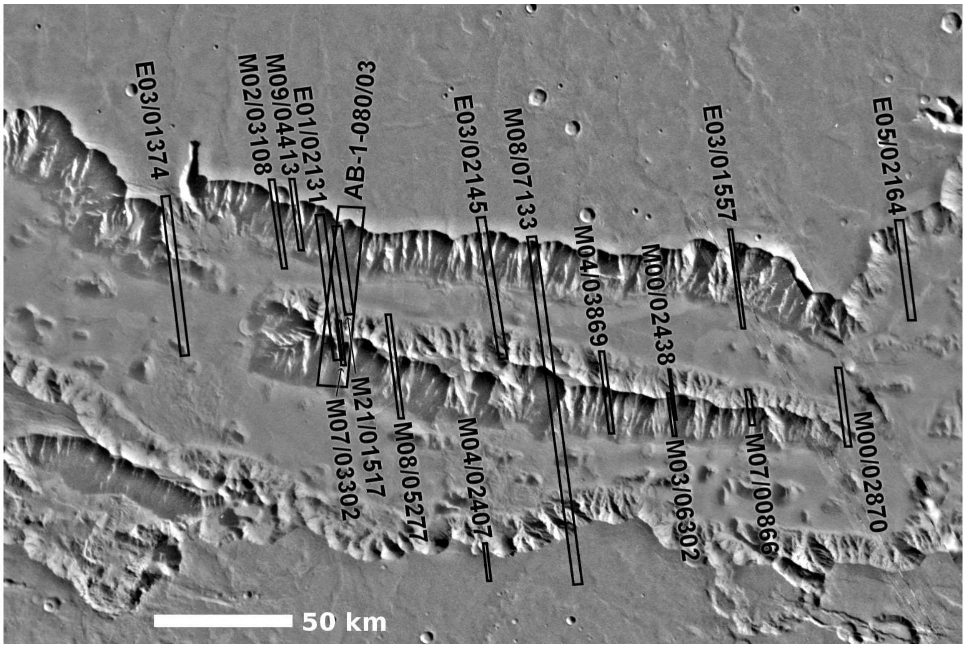

Figure 1: Mars Digital Image Mosaic (MDIM2.1) (Archinal et al., 2003; Kirk and Lee, 2005) of Viking orbiter data showing the primary study area of eastern Coprates Chasma. Locations of MOC narrow-angle images used in this study are indicated by their outlines.

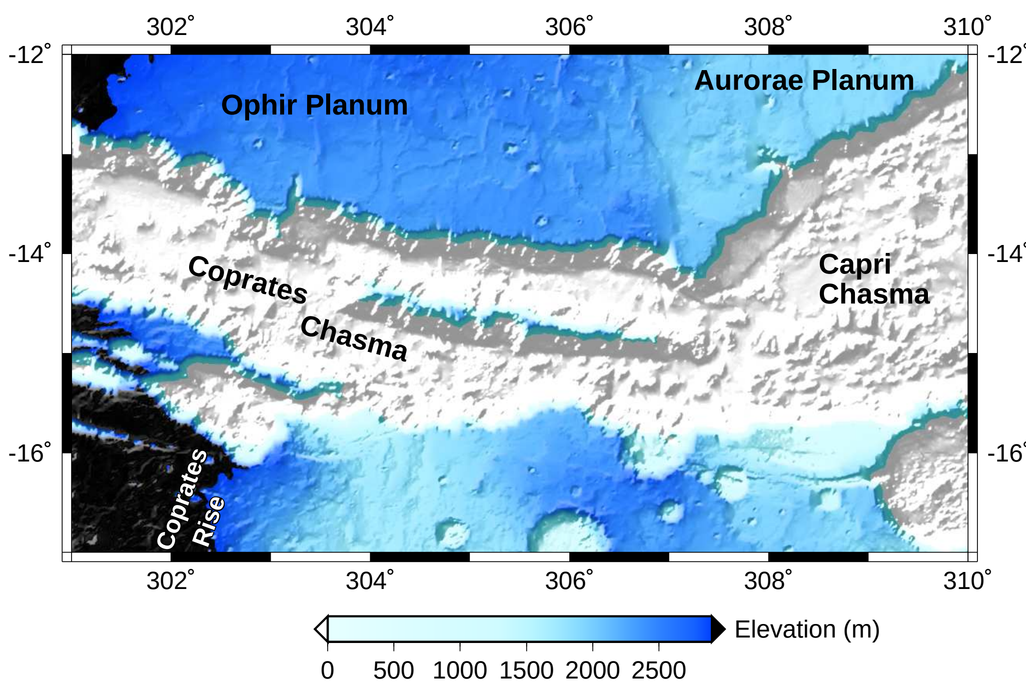

Figure 2: Elevation map of eastern Coprates Chasma created from the 1/128th degree MOLA gridded data.

1 Introduction

The Mars Orbiter Camera (MOC) (Malin et al., 1992; Malin and Edgett, 2001) on-board the Mars Global Surveyor (MGS) spacecraft has observed extensive layering near the martian surface and in the Valles Marineris system (e.g. McEwen et al., 1999; Malin and Edgett, 2001). Layering exposed in the walls of terrestrial canyons is often sedimentary in nature, with new layers having been deposited from rivers, lakes, or oceans. Alternately, volcanic processes with multiple episodes or pulses of activity can deposit many layers of volcanic rocks and/or tephra, and intrusive magmatism can also create layered sequences at depth that are later revealed by erosion and uplift. The Valles Marineris is the only feature that cuts down over 9 km into the martian crust. The origin of the layers is unknown, but there are hypotheses for both fluvial sedimentary (e.g. Malin and Edgett, 2000) and volcanic origins (e.g. McEwen et al., 1999; Williams et al., 2003). Even diagenetic processes have been proposed (Treiman et al., 1995). Also relevant to the exposures that we see today are the formation processes of the giant chasma system itself (e.g. Sharp, 1973; Tanaka and Golombek, 1989; Schultz, 1991; Lucchitta et al., 1992, 1994; Peulvast et al., 2001; Mège et al., 2003) and what geologic changes the region has gone through since these chasmata opened.

Layering can be seen in the high-resolution MOC images, and correlated with particular heights from individual Mars Orbiter Laser Altimeter (MOLA) (Zuber et al., 1992; Smith et al., 2001) tracks. In addition to the tracks that were acquired simultaneously with many MOC images, there are a number of MOLA tracks that criss-cross an area not tied to any particular image. Thermal Emission Imaging System (THEMIS) (Christensen et al., 2004) infrared multi-band images at 100 m/pixel and visible wavelength images at 18 m/pixel are useful for tracing layers, and for constraining their thermo-physical properties (emissivity and thermal inertia).

We examined layering seen in the eastern portion of Coprates Chasma (Figs. 1, 2) and the north rim of Capri Chasma (Fig. 3). We estimated individual layer thickness, measured the thickness of layered units, and measured the horizontal extent and elevations of layer outcrops. Layers are identified in several MOC and THEMIS images to determine how far they extend along the chasmata. This mapping allows us to determine if the layers are flat-lying or if they dip down in a particular direction over large distances. Lacustrine or deep oceanic deposits should be horizontal unless they have been tectonically tilted, in which case the tilted layers should have a systematic relationship to regional tectonics. Air-fall ash or dust will drape over pre-existing topography. Wind-blown sand will pile up against topographic obstacles. Lava flows will be largely but not entirely horizontal. Horizontal layers may also be interbedded lavas, tephra, and sediments.

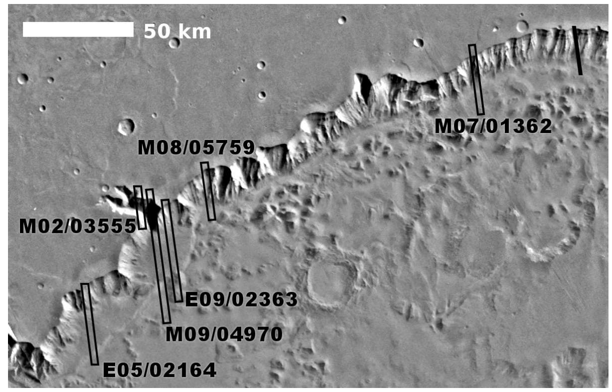

Figure 3: Viking mosaic (MDIM2.1) showing the Capri Chasma rim and Aurorae Planum above it. The locations of MOC narrow-angle images that were used in this study are indicated by the outlines.

We begin with a brief description of the method we used to obtain the layer elevations (Section 2). We then state the observations that we made of the massif, the chasmata rims, and chasmata slopes (Section 3). Finally, we discuss these observations (Section 4) and our conclusions (Section 5).

2 Layer elevation measurement

Obtaining an accurate measurement for the elevation of an outcrop of thin ($\sim$ 10 m thick) layers with MOLA data cannot be done by simply reading off the elevation of individual MOLA shots. MOLA footprints are 168 m in diameter (Smith et al., 1999a) and have center-to-center spacings of about 300 m. This means that a MOLA shot, even if it happens to fall directly on a thin layer is also sampling the elevations above and below that layer. However, these layers often sit above constant slopes

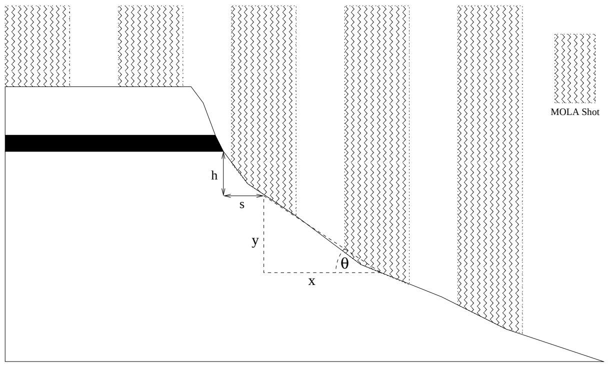

Figure 4: Sketch showing an example cross-section at the top of Eastern Coprates Chasma and the way that MOLA measurements intersect with the surface. It illustrates how we obtain an elevation measurement for the outcrop of the thin dark layer. See Section 2 for an explanation of the symbols.

with many MOLA shots on it (Fig. 4). We can get a measurement of the absolute elevation of the thin layer by using the equation $h = s \tan\theta$, where h is the difference in elevation between the elevation of the layer and the elevation of the center of the MOLA shot just below the layer, s is the plan form distance between the center of the MOLA shot just below the layer and the layer itself, and θ is a measurement of the slope. This method works even if the orientation of the MOLA track is not perpendicular to the strike of the layer outcrop as long as s is measured along the direction of the MOLA track.

This measurement estimate breaks down if there is a severe change in slope just above the highest MOLA shot on the slope. With the shot as far down the slope as possible (maximum s given shot spacing), a ten degree slope difference yields a maximum error in elevation of about 30 m. This error linearly decreases with the value of s, which is different for each measurement. In practice we think that this error is on the order of meters for our measurements.

When we quote an elevation measurement in this study, it is based on the MOLA equipotential topography (Smith et al., 1999a). These elevations are the planetary radius (the distance from the center of Mars to the point on the surface) minus the areoid radius (the radius of the reference areoid with a 3396 km mean equatorial radius).

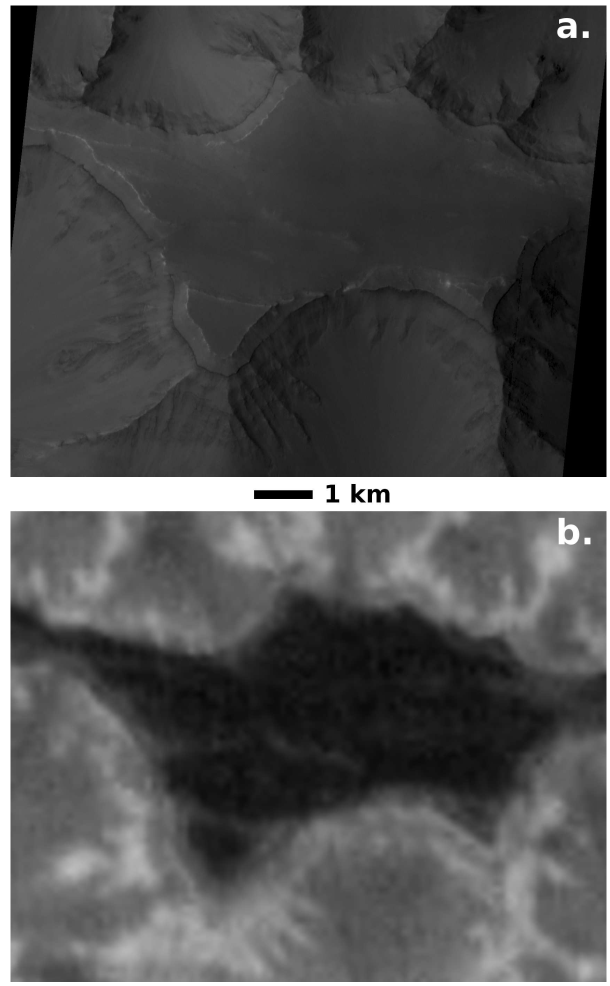

Figure 5: Context images for the westernmost flat-topped area on the massif in eastern Coprates Chasma. (a) MOC image AB-1-080/03, 4.7 m/pixel. (b) THEMIS nighttime IR image I00820002 (band 9), 100 m/pixel. All images in this study are displayed with north to the top.

3 Observations

3.1 Massif in eastern Coprates Chasma

A large massif in eastern Coprates Chasma is situated closer to the north wall of Coprates Chasma than the southern wall, near where the Valles Marineris widens into Capri Chasma (Figs. 1 and 2). It is located near 15° S, between 304° and 307° E. MOC images display spur-and-gully mor-

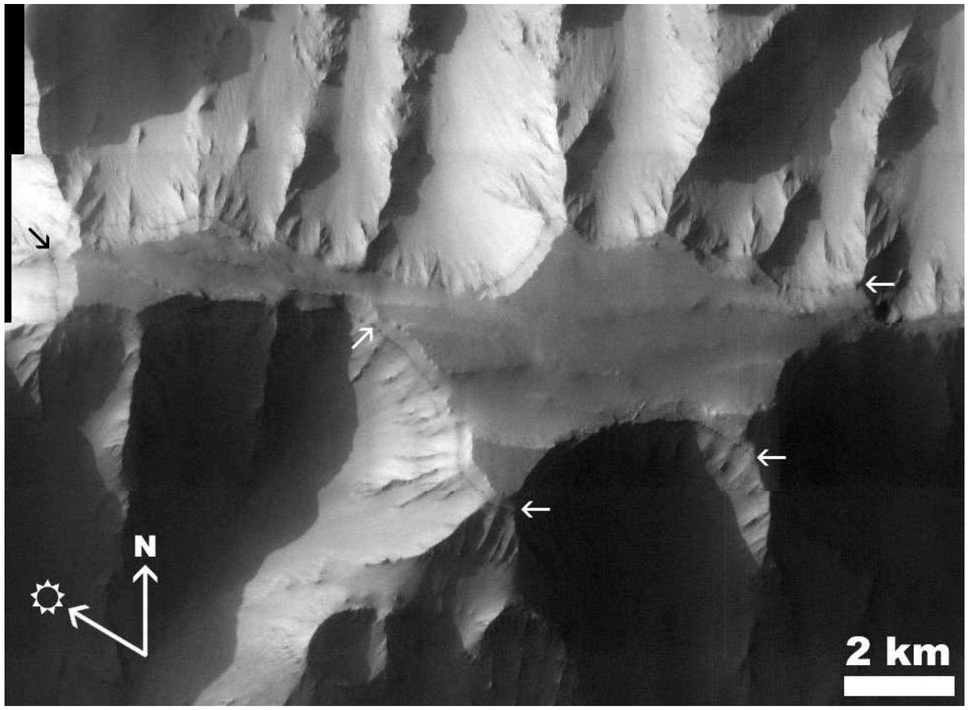

Figure 6: THEMIS VIS image V03810003, showing the westernmost flat-topped area of the massif in Coprates Chasma and a dark, competent layer below the level of the flat top. This layer can clearly be seen, even on sunward-facing slopes, demonstrating that it has a lower albedo. This dark layer is indicated by arrows.

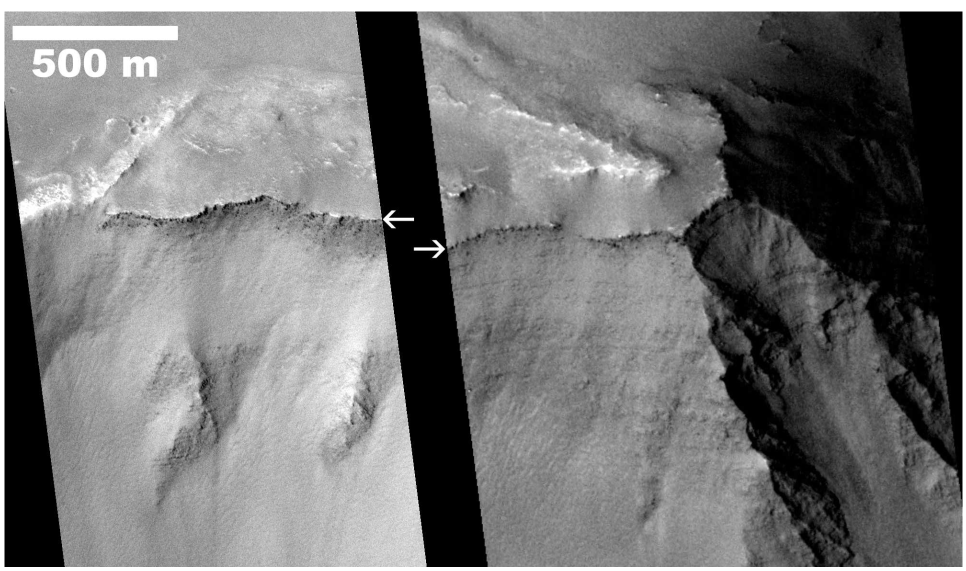

Figure 7: MOC images showing the cliff-forming layer near the top of the flat-topped areas on the massif. In both images, the south face of the massif slopes down towards the bottom of the image. Image M07/03302 on the left and image M08/05277 on the right are separated by about 22 km.

Elevations of Competent Layer Outcrops

MOC Image	MOLA Orbit	Elevation (m)	E Longitude	Latitude
Massif Outcrops				
AB1/08003	12359	1895 (N)	304.16	-14.40
		1905 (S)	304.17	-14.46
M08/05277	12774	2034	304.50	-14.56
M04/03869	12120	2160	305.86	-14.74
M03/06302	11793	2180 (N)	306.25	-14.78
		2130 (S)	306.25	-14.79
M00/02438	10460	2130	306.27	-14.79
North Rim Outcrops				
M09/04413	13101	2273	303.88	-13.61
E03/02145	19526	2300⋆	305.12	-13.77
M08/07133	12862	2330	305.36	-13.83
E03/01557	19438	2409⋆	306.76	-13.87

Table 1: Measurements in order from west to east. They show the MOC image and the MOLA track that was paired with it to yield the elevation. M03/06302 and M00/02438 are very near one another.
⋆ These measurements have an error on the order of 100 m because these MOLA tracks have pointing uncertainties that make precise alignment with their MOC images difficult.

Layer Apparent Dips

MOC Images	Distance (km)	Apparent dip (°)	Dip direction
Massif			
AB1/08003 & M08/05277	20	0.39	West
M08/05277 & M04/03869	78	0.09	West
M04/03869 & M03/06302	23	±0.05	West
AB1/08003(N) & AB1/08003(S)	4	0.00	North
M03/06302(N) & M03/06302(S)	0.61	3.65	South
AB1/08003 & M03/06302	122	0.13	West
North Rim			
M09/04413 & M08/07133	60	0.04	West

Table 2: These apparent dip measurements are in order from west to east along the massif between the measured elevations in Table 1. The last massif apparent dip is from the westernmost measurement to the easternmost. The ±0.05° measurement is for the apparent dip between the outcrop in M04/03869 and either the north outcrop in M03/06302 (+0.05°) or to the south outcrop (−0.05°). The apparent dip between the north and south outcrops in AB1/08003 is zero for the number of significant figures in the above table.

phology and layers on the massif that are very similar to the chasma wall rock. The massif appears to be compositionally and structurally similar to the chasma wall rock as well (Frey, 1979; Schultz, 1991). This massif has a few flat-topped areas along its roughly 230 km length (Fig. 5). The flat-topped areas along the spine of the massif are most likely the remnants of the plains surface that covered this area prior to the opening of Coprates Chasma.

Just below the level of those flat-topped areas on the massif and in other places along the crest of the massif, a distinct, dark-toned layer can be seen (Fig. 5a), even in sunward facing slopes (Fig. 6). Figure 7 shows higher resolution images highlighting this resistant cliff-forming unit which crops out below the flat-topped surfaces. Since this layer can be seen everywhere along the edge in Fig. 6, and a layer with a similar expression and morphology is observed 22 km farther east (Fig. 7), we think that it may be extensive. In fact, there are several MOC images along the massif where a layer with very similar characteristics is exposed (Table 1).

The elevation measurements of this topmost strong layer (Table 1) allow us to estimate the apparent dip of this layer. We assume that the layer was originally horizontal (see Section 4.1 for why we think that this is a reasonable assumption). We can measure apparent dips in two general directions (Table 2). The massif is oriented roughly east-west, with its general trend about 10° north of west, and we have several measurements of the layer outcrop along it. In a few places the layer is exposed on both the north and south faces of the massif, allowing us to measure a few apparent dips in a more north-south direction (Fig. 8).

An example of north-south extension can be seen on the westernmost flat-topped area of the massif. MOC image E01/02131 (Fig. 9) shows the strong layer about a hundred meters below the flat-topped level of the massif, and a 420 m long segment that dropped about 70 m. This measurement is based on extrapolations of the elevations of the topmost strong layer in this area. Given the length of the segment, the width of the gap in the layer above, and the 70 m of down-drop, we find that the normal faults which bound this down-dropped block have fault angles of 60°, consistent with normal faults on the Earth. The layer isn't the only thing showing that there is a down-dropped block here, MOC and MOLA data also show a shallow depression (60 m deep above the down-dropped layer exposure) which probably indicates the extent of this block. Unfortunately, there are no MOC images to help determine

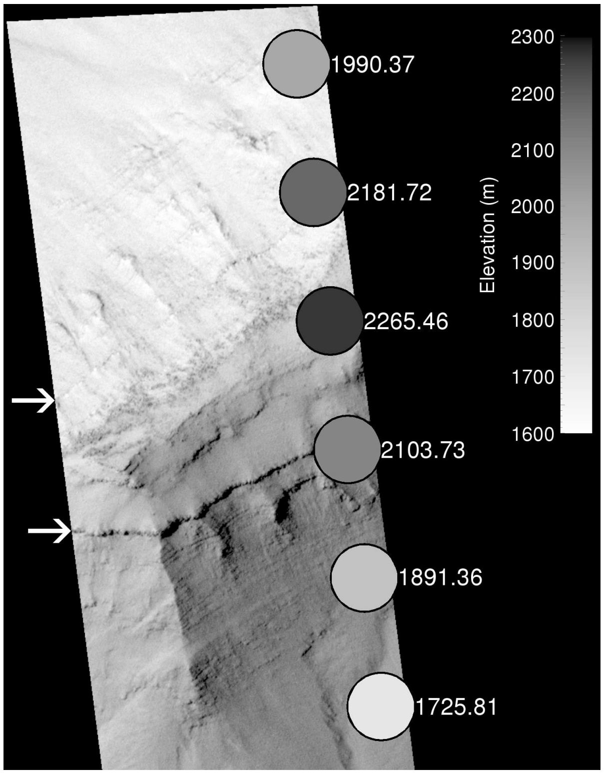

Figure 8: Portion of MOC image M03/06302, with the MOLA data from the track that was acquired simultaneously with the image plotted on top. The size of the circles is the approximate size of the MOLA footprint (168 m diameter). This image covers the crest of the massif, and the white arrows point to the outcrops of the topmost competent layer on both sides.

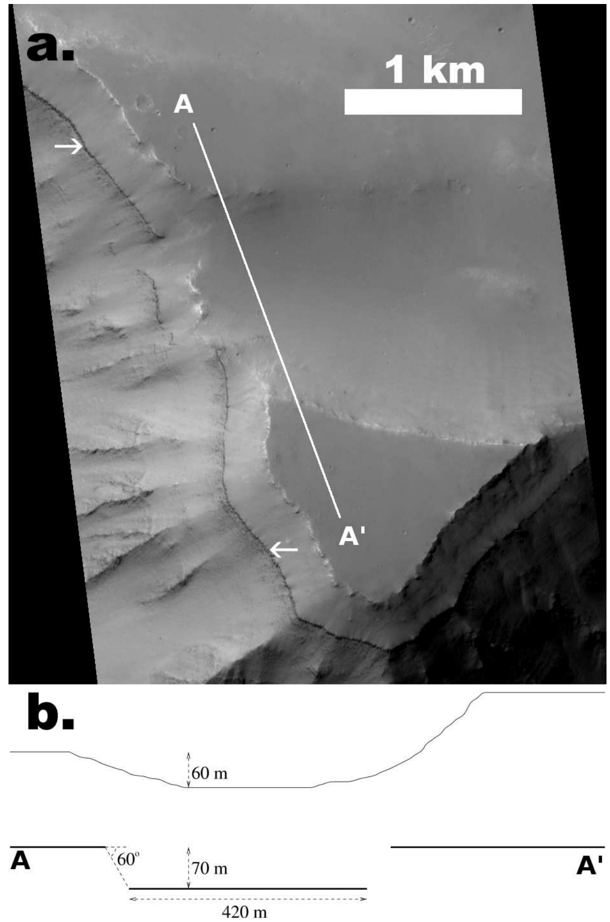

Figure 9: (a) Portion of MOC image E01/02131 showing a closeup of the westernmost flat-topped area shown in Fig. 5a. The white arrows indicate the topmost strong layer. (b) This schematic illustrates the down-dropped block as seen from the west along the A-A' line (top profile is the surface, straight lines below it represent the dark layer). It shows that the dark layer exposed on the western facing slope has a 420 m long segment that is about 70 m in elevation below the level of the majority of the dark layer. Distances and elevations derived from MOC and MOLA data.

the eastern extent of this block.

The topmost strong layer is the most easily identifiable layer in the stack due to its visual contrast and high apparent strength. However, other resistant layers can be identified below it. The next lower exposure of competent layers is part of a sequence at least 200 m thick. It is difficult to determine if this sequence is varying in thickness from place to place or if it is partially buried by talus. This sequence also contributes to the steep slopes near the crest of the massif and supports a topographic bench in MOC image M08/05277 (Fig. 10). Unlike the distinct topmost layer, this unit appears to be a sequence of more resistant layers, and while not as dark as the topmost competent layer, it does have a slightly darker tone than surrounding weak layers.

The western exposures of this topmost layer and next most competent unit appear to have a 100 m thick sequence of slightly lighter-toned thinly bedded materials between them. However, M03/06302 and M00/02438 (in the eastern part of the massif)

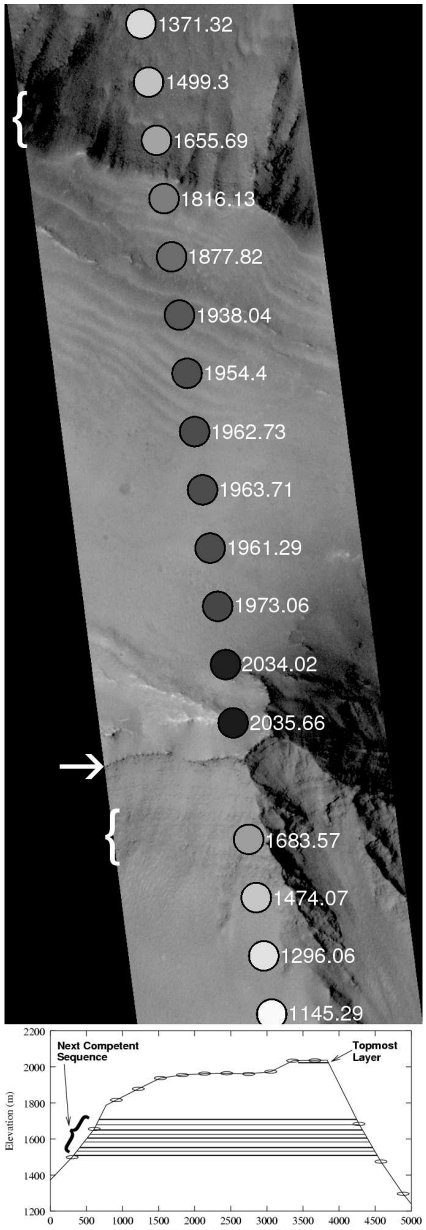

Figure 10: Portion of MOC image M08/05277 overlain with MOLA track 12774, north is to the top. Slopes are locally steepened by the presence of the topmost dark layer (indicated by an arrow on this image). Stratigraphically lower is a topographic bench. This bench appears to be supported by the next most competent sequence of layers (visible on both the north and south sides of the massif as indicated by the brackets). Schematic at the bottom gives a view from the west, north is to the left, and the vertical exaggeration is 2.5.

do not show such a gap between these two units. The gap between these units is identified by slope morphology and a slight change in tone between the intervening weak layer and the next competent unit. To determine whether these strata represent thinning and thickening units, a true unconformity, or if we are not correctly interpreting these exposures will require more coverage.

Other competent layers are seen farther down the stratigraphic stack but are more difficult to discern due to the amounts of talus that mantle the slopes. These lower competent units are evident in occasional spurs or ridges that crop out from the talus mantle on the slopes. However, it is difficult to correlate these layers along the chasma slopes because they are not seen everywhere at a particular elevation due to the spur-and-gully morphology of the slopes, and the differential accumulation of talus at different locales.

3.2 Coprates Chasma slope, north of massif

The topmost strong layer observed in the massif is also evident directly north of the massif in the north rim of Coprates Chasma (see Table 1). Unfortunately, due to small pointing errors in the MOLA dataset, only two of these four MOC images can be precisely aligned with their MOLA tracks. The two good outcrops yield a 0.04° slope down to the west (Table 2). Our estimates for the elevations of the other outcrops are consistent with this slope as well. These measurements indicate that the topmost strong layer in the north rim of Coprates Chasma is flat-lying relative to the layer in the massif. The outcrop elevations here are higher than in the massif (Fig. 11).

The next unit of strong layers seen to crop out below the topmost strong layer in the massif is also evident here on the north rim of Coprates Chasma (Fig. 12), where it is not obscured by talus on the slope. Again, it appears to be 100 to 200 m thick, but seems to be about 200 m stratigraphically below the topmost strong layer.

The topmost strong layer is modified by a 7.5 km diameter crater perched near the edge of the plateau that is sectioned by the chasma (Fig. 13). The layer is observed in the chasma rim to the east and west of the crater. Therefore the bowl of the crater should intersect the layer, however it is not immediately apparent. A thin, bright layer can be seen in the

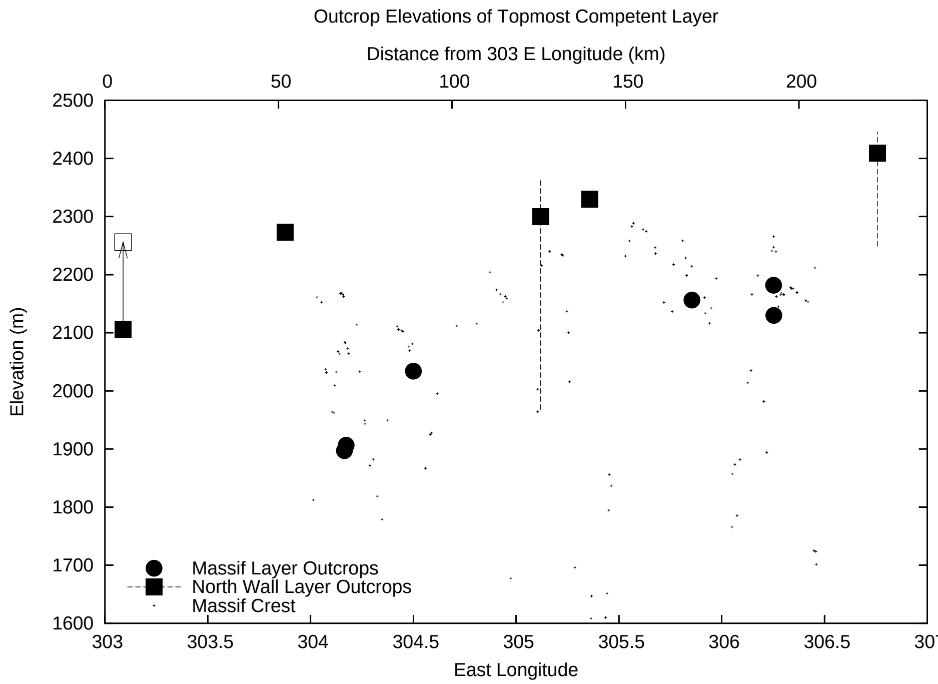

Figure 11: East longitude of the topmost strong layer outcrop locations and their elevations both in the massif and in the north rim of eastern Coprates Chasma are shown. The elevations of the crest of the massif are also plotted to show the variability of the massif crest in relation to the layer outcrops. The westernmost north rim data point has an arrow which points to the estimated elevation of the layer in this location prior to the 150 m down-dropping of this portion of the plateau (see Sections 3.4 and 4.1 for details). The error bars on the other two data points result from imperfect pointing information which prevents accurate MOC/MOLA alignment for these outcrops.

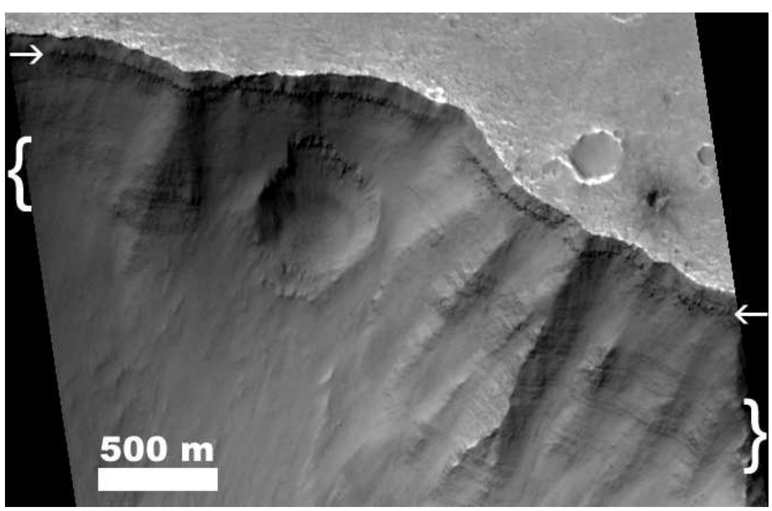

Figure 12: Portion of MOC image E03/02145. Arrows indicate the location of the topmost strong layer just below the plateau surface. Brackets indicate a competent sequence of darker-toned layers.

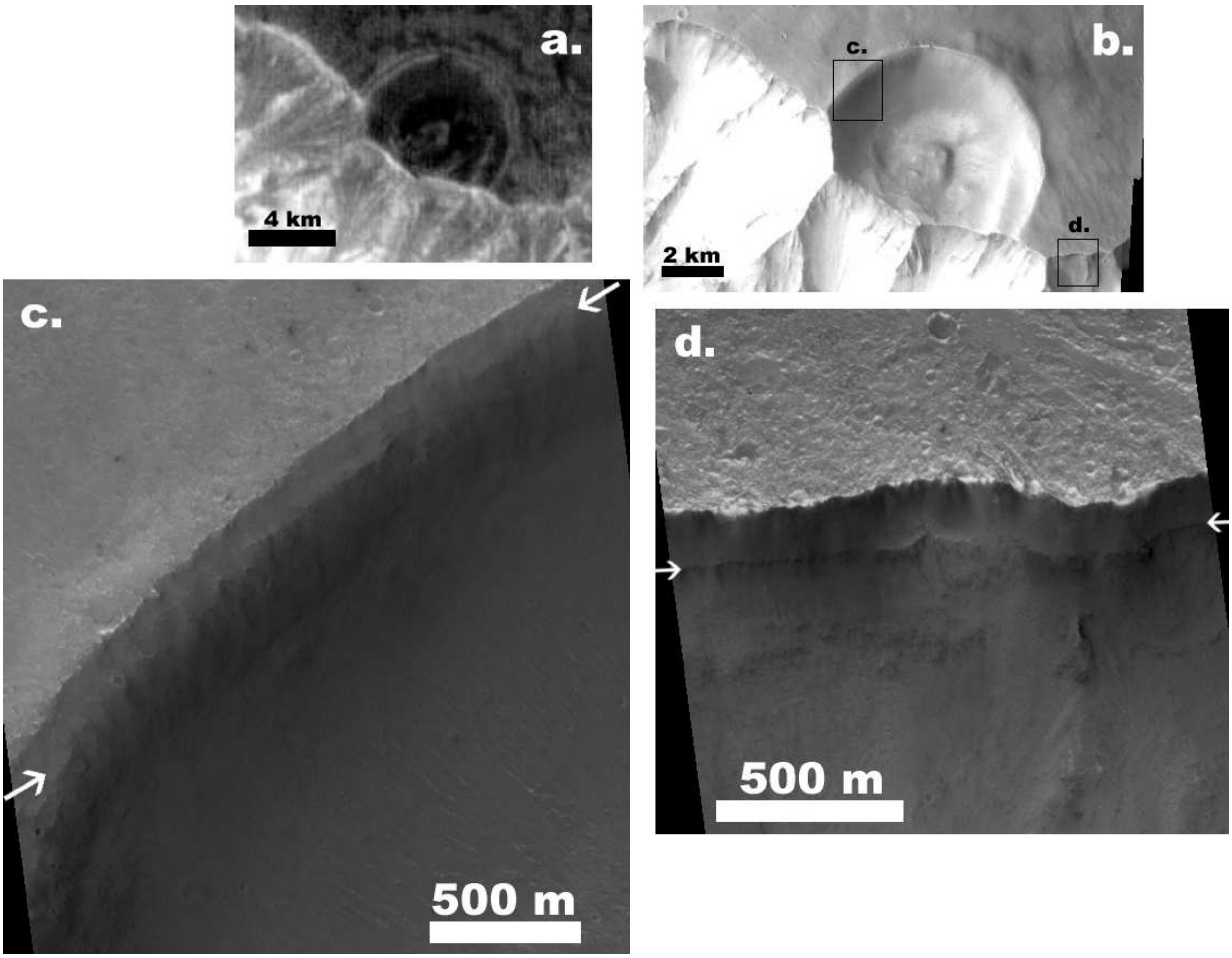

Figure 13: The topmost strong layer is interrupted by a crater, but is seen on either side of it on the chasma slope, and may be present within the bowl of the crater itself. (a) Portion of THEMIS nighttime IR image I07486008. The bowl of the crater is dark and therefore has a lower temperature relative to the surrounding terrain. These temperatures may mean that there is more lower-thermal-inertia dust within the crater than outside. However, a bright layer can be seen within the bowl of the crater that could correspond to the topmost strong layer. (b) Portion of THEMIS VIS image V06831002, the black boxes show the locations of c and d. (c) Portion of MOC image M02/03108. A faint hint of a break in the slope of the crater 75 m in elevation below the rim height, the arrows indicate this slope break. Slope break may be the expression of the topmost layer in the crater. (d) Portion of MOC image M09/04413. The topmost strong layer is evident here below a 100 m thickness of weaker materials.

nighttime THEMIS data (Fig. 13a) in approximately the expected location within the crater. Arrows in Fig. 13c point out an apparent break in slope on the crater wall. This break in slope is 75 m in elevation below the rim of the crater, but 130 m above the elevation of the topmost competent layer as observed in M09/04413 (Fig. 13d). The rim of the crater is about 100 m above the surrounding plateau. If that is how much the stratigraphy here has been uplifted because of the impact, then this break in slope may indeed be the topmost competent layer uplifted by the impact.

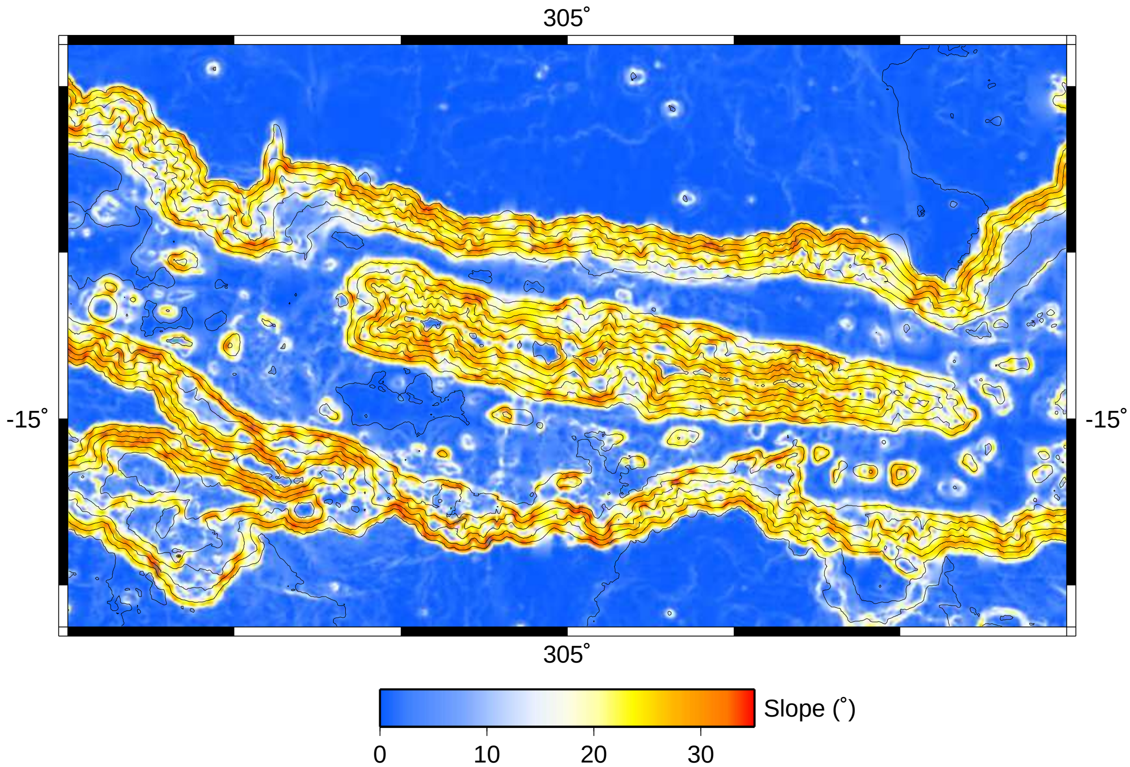

Figure 14: Slope map created from 1/128th degree gridded MOLA data. The elevation contours are every 1000 m.

3.3 Coprates Chasma slope, south of massif

The rim of Coprates Chasma directly south of the massif has a very different character from that directly to the north of the massif and the slopes of the massif itself. Schultz (1991) noted a structural difference between the north and south slopes of Coprates Chasma in general. There is also a difference between the the southern rim and slope of this easternmost section of Coprates Chasma from that farther west. The plateau beyond the south rim here is just east of the Coprates rise (Fig. 2) into which are carved the Nectaris Fossae farther south. This broad anticline separates the higher Thaumasia Planum to the west from the lower-lying Noachis Terra to the south and east of Valles Marineris. Therefore the character of the greater plateau geography south of the rim here is different than that farther west towards Tharsis.

The differences between the north and south rims of Coprates Chasma are highlighted by high-resolution images and topography. MOLA data indicate that the range of surface slopes is similar on the slopes of Coprates Chasma both north and south of the massif, as well as on the massif itself (Fig. 14). The trend of the chasma's rim to the south is more irregular and scalloped by large landslide alcoves than on the north rim of the chasma in this region. Along the northern slope, the ridges in the spur-and-gully morphology have a roughly regular wavelength from 1.5 to 5 km. The south slope displays two characters: to the west, it is dominated by large landslide alcoves, whose bounding spurs have a

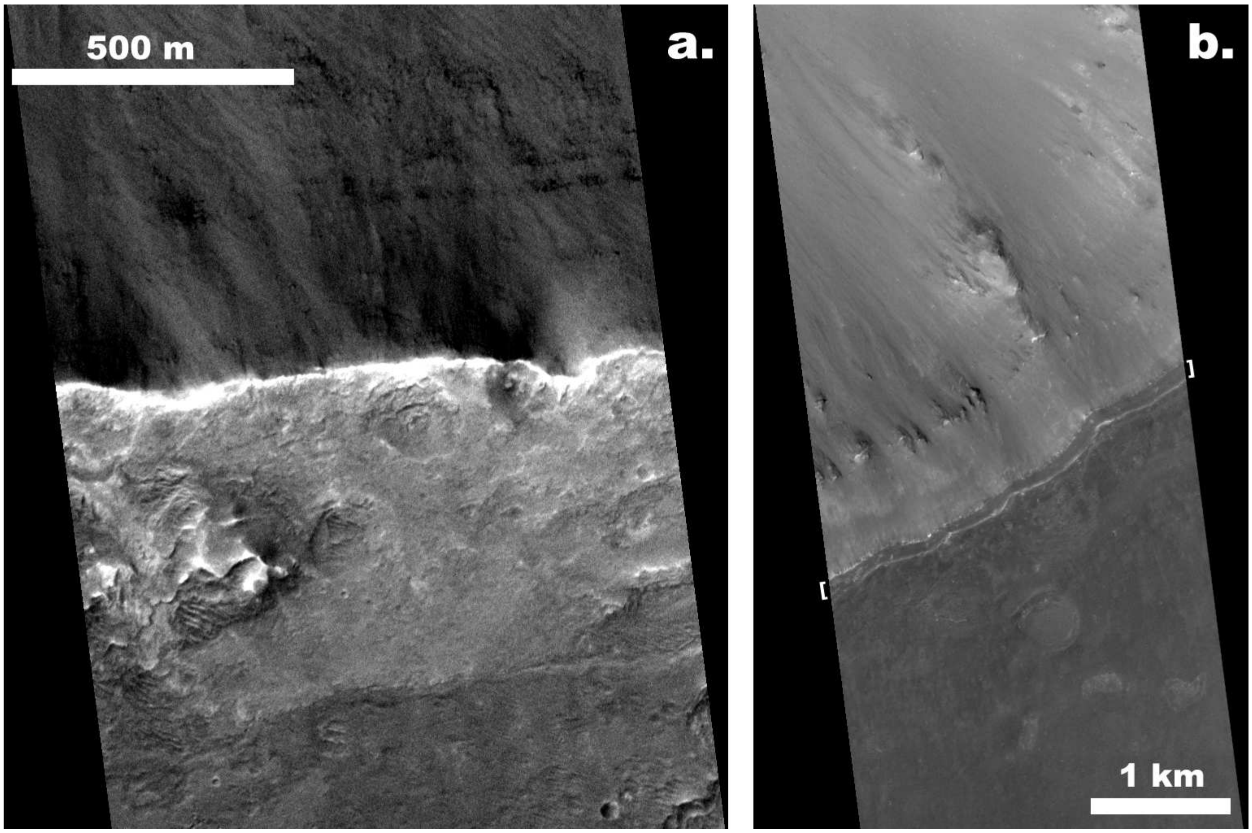

Figure 15: Image portions covering the the south rim of Coprates Chasma south of the massif. (a) M04/02407. No topmost dark, strong layer evident, but the plateau surface seems indurated. (b) M08/07133. This image shows that there is a layer that has retreated back 80 to 120 m from the plateau edge (indicated by brackets) Based on MOLA elevation data, this layer is 30 to 40 m thick.

wavelength from 5.5 to 6.5 km; to the east, the slopes are not dominated by landslide alcoves, and show a more regular spur-and-gully morphology with a spur wavelength similar to that of the north slope.

These gross differences in slope morphology are not the only differences between the east and west portions of the slope of Coprates Chasma south of the massif. The elevation of the plateau along the north rim of Coprates Chasma maintains a relatively constant elevation along the 230 km length of the massif. However, the plateau along the south rim varies from 600 m below the elevation of the north rim in the west to nearly the same elevation as the north rim in the east (Fig. 2).

Although portions of the southern plateau edge have higher elevations than the summit of the massif, no evidence of the topmost dark competent layer can be seen along its length. Here, the rim does not show cliff-forming layers although such sequences are observed farther down-section (Fig. 15).

The MOC coverage along the south rim is quite sparse, and so there may be an observational bias, but there are only occasional outcrops of competent units below the plateau surface along the slopes, and we cannot correlate them to other outcrops along the south slope, nor to those within the massif or north slope.

3.4 Coprates Chasma slope, west of massif

On the north rim, west of the area where the crater is sectioned by the chasma slope (Fig. 13), a re-entrant cuts northwards into Ophir Planum (Fig. 16), and

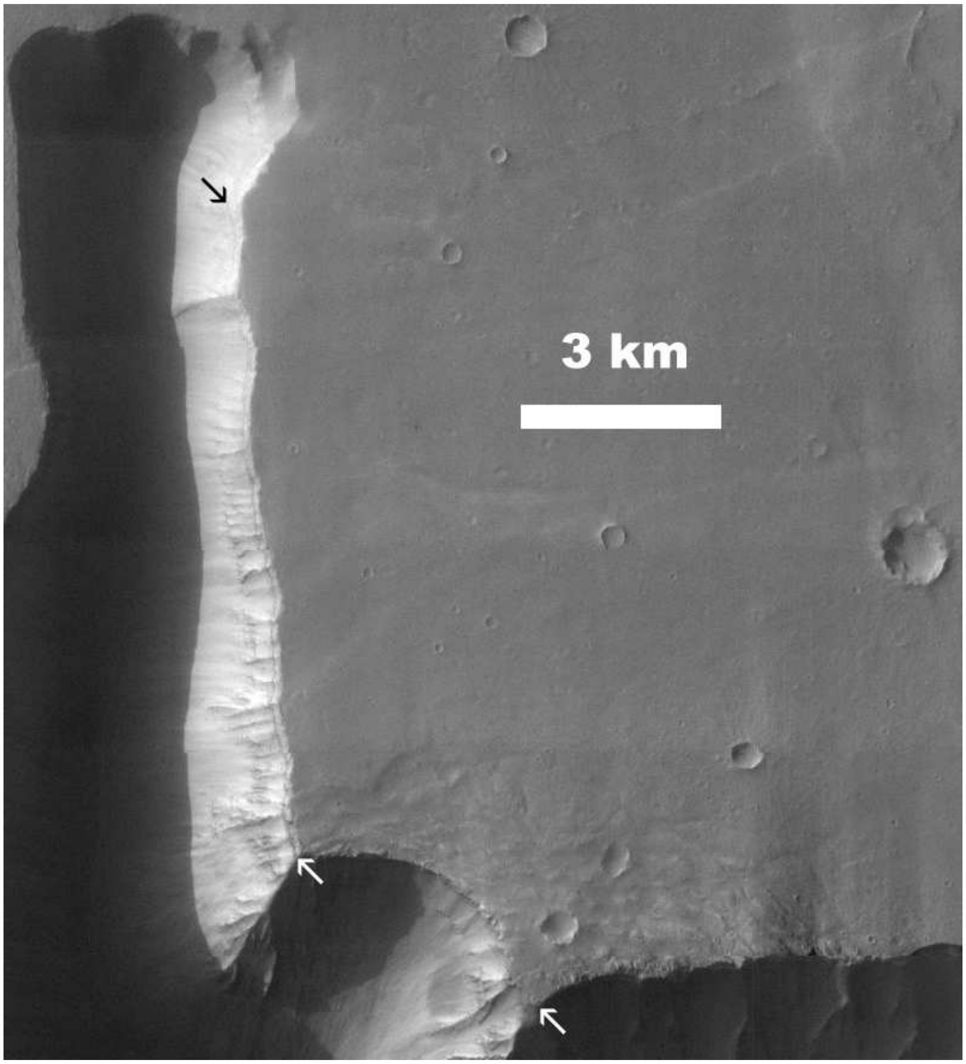

Figure 16: Portion of THEMIS VIS image V03835003. The context for this image is in Fig. 17d. A small chasm that cuts north into the southern Ophir Planum surface to the northwest of the massif in Coprates Chasma can be seen. A dark layer can be seen in the sunlit eastern slope just below the cliff edge (indicated by arrows).

the dark layer is visible on the west-facing slope in the afternoon sunlight.

Farther west a promontory near 303° E, 13.5° S juts south into the chasma (Fig. 17). The plateau surface of this promontory shows east-west linear depressions, and a slight drop in elevation, which led Witbeck et al. (1991) to mark a normal fault in this area. MOC image E03/01374 (Fig. 17c) shows the topmost layer cropping out here. In this area instead of an even stack of material above the strong layer, there are hills or hummocks from 500 m to 1 km in diameter. The elevation of the topmost strong layer here is 2106 m, 167 m lower than the elevation 45 km to the east. MOLA data show that the plateau surface at the south edge of the promontory is about 150 m lower than the plateau surface north of the fault zone. If the layer here was down-dropped a similar amount, then the pre-fault elevation of the layer here is consistent with the elevation of the layer in the chasma slope north of the massif (Fig. 11). In

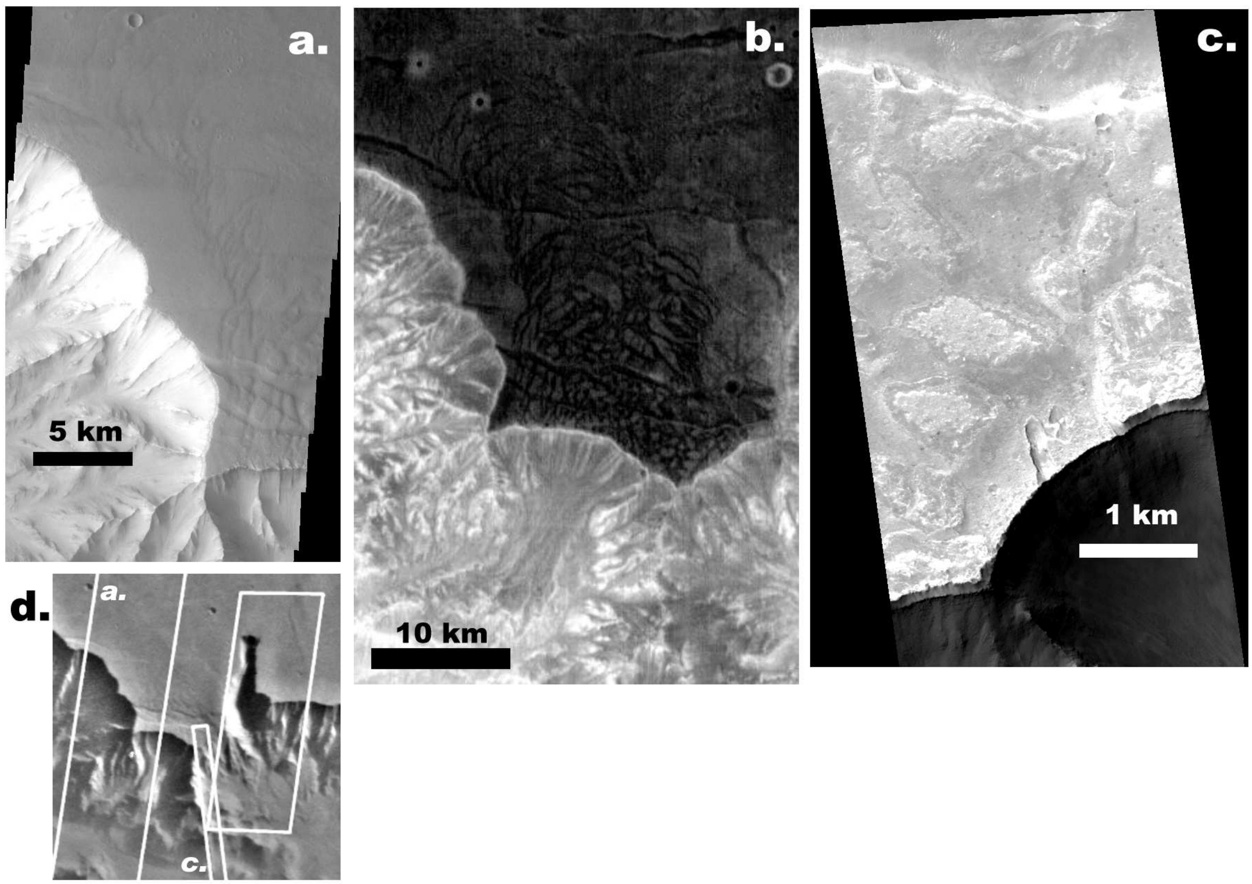

Figure 17: Promontory on N rim jutting out into Coprates Chasma just west of the massif. (a) Portion of THEMIS VIS image V06856002. The topmost dark layer can be seen just below the plateau surface along the slopes to the west and along the south of this promontory. Additionally, the hummocky surface texture of the promontory can be seen here. (b) Portion of THEMIS nighttime IR image I08235013. This image highlights the relative temperature differences at night between the hummocks and the lanes between them. (c) Portion of MOC image E03/01374. This image shows the topmost strong layer that underlies the hummocky surface here. (d) MDIM2.1 context image shows the outlines of the whole images for a and c. The unlabeled outline is that of THEMIS VIS image V03835003 (Fig. 16).

addition to being evidence of the extent of the layer, this outcrop also displays how normal faulting has modified the layer.

Farther west from the immediate area of the massif, coverage decreases, and identification of the topmost strong layer becomes more difficult. MOC image E02/01171 (Fig. 18) displays a resistant layer, but the material above it has retreated back from the edge by 100 to 200 m (MOLA indicates that the thickness of that layer is only 10 m). The elevation of the resistant layer is 2787 m, roughly 500 m above the elevations of the topmost resistant layer north of the massif. MOC images farther west along the Coprates Chasma north rim also show a resistant layer just below the plateau surface. If it is all the same layer, its elevation mimics that of the plateau surface (the layer is observed either at the elevation of the plateau surface or tens of meters below it) as it rises up above 5000 m and then descends back down where Coprates Chasma meets Melas Chasma to the west (Fig. 19, Table 3).

It is difficult to tell if these outcrops of resistant rocks that form a distinct break in slope between the plateau surfaces and the slopes are all part of the

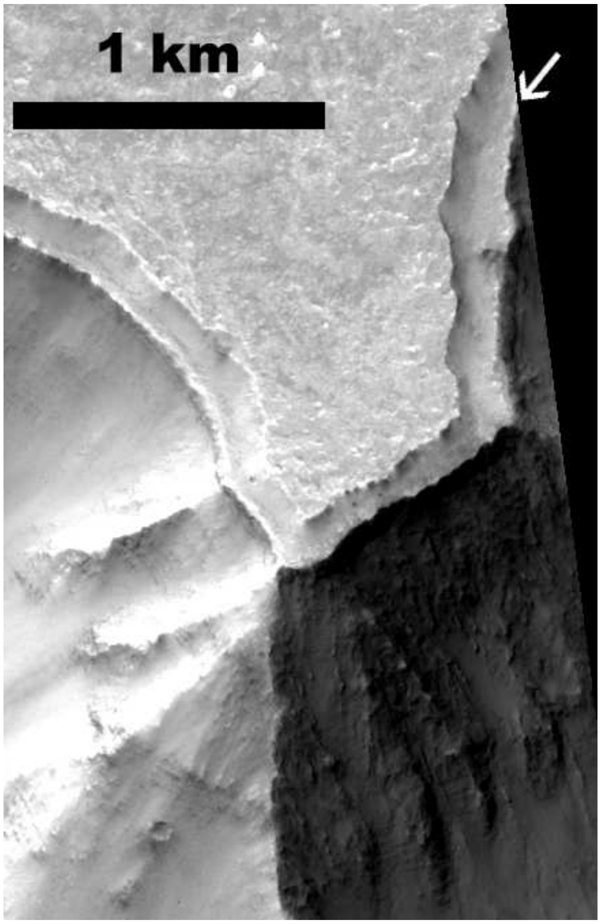

Figure 18: Portion of MOC image E02/01171 showing how the material that overlies the resistant layer (indicated by the arrow) has retreated 100 to 200 m back from that edge. MOLA data indicate the layer is ~ 10 m thick.

Outcrop Elevations West of Massif

MOC Image	MOLA Orbit	Elevation (m)	E Longitude	Latitude
E02/02151	19137	4075	291.02	-9.76
M12/02722	14359	4950	293.79	-10.95
M08/06016	12812	5140	296.32	-11.52
M10/03722	13642	5050	297.32	-11.75
E02/01171	19011	2787	301.60	-12.84

Table 3: These measurements are in order from west to east. They show the MOC image that the MOLA track was matched with to yield the elevation measurement of the competent layer that is present on the rim.

same topmost resistant strong layer observed north of the massif in eastern Coprates Chasma. The high-resolution coverage is sparse, which makes lateral continuity of the layers difficult to establish.

Figure 19 shows the locations of outcrops of the topmost competent layer where we were able to positively identify it in MOC and THEMIS VIS images in eastern Coprates Chasma.

3.5 Capri Chasma slope

Where Witbeck et al. (1991) show the boundary between the Hr and Hpl_3 units, roughly coinciding with the boundary between Ophir Planum and Aurorae Planum (Figs. 2 and 20), we note an additional elevation difference between the two plana and a difference in chasma rim morphology. North of the massif in Coprates Chasma, that rim is marked by the presence of the topmost competent layer supporting a stack of presumably weaker overburden materials that form the edge of the plateau. East of this Ophir/Aurorae boundary, where the MOC images show a sharp edge, that rim appears to consist of a stack of resistant layers, rather than showing a distinct, single layer. The elevations of the top of this stack are consistently 200-300 m below the elevation of the topmost competent layer north of the massif in Coprates Chasma. An example of this is in E05/02164 (Fig. 21).

A small tributary chasma (Fig. 22) cuts into the side of Capri Chasma (Fig. 3) near 308° E, 13° S, and displays more of its stratigraphy. M02/03555 (Fig. 23) shows a detail of the north rim of this tributary chasma cutting into the plateau surface (which is at 1820 m). A unit of cliff-forming layers can be seen on the north rim of the tributary chasma, and the corner where a short, theater-headed depression intersects the tributary chasma. However, the expression of this unit disappears northward along the eastern rim of that shallow depression. The depression's depth appears to be limited by a unit that crops out from 1050 m to 700 m elevation in the tributary chasma. The morphology of the depression indicates that it was perhaps a channel formed by sapping into the massive layer. If so, this would indicate that perhaps that unit is not only relatively stronger, but also potentially an aquitard. Just slightly farther east, M09/04970 (Fig. 24) also covers the north rim of the tributary chasma, showing a competent unit around 1750 m elevation.

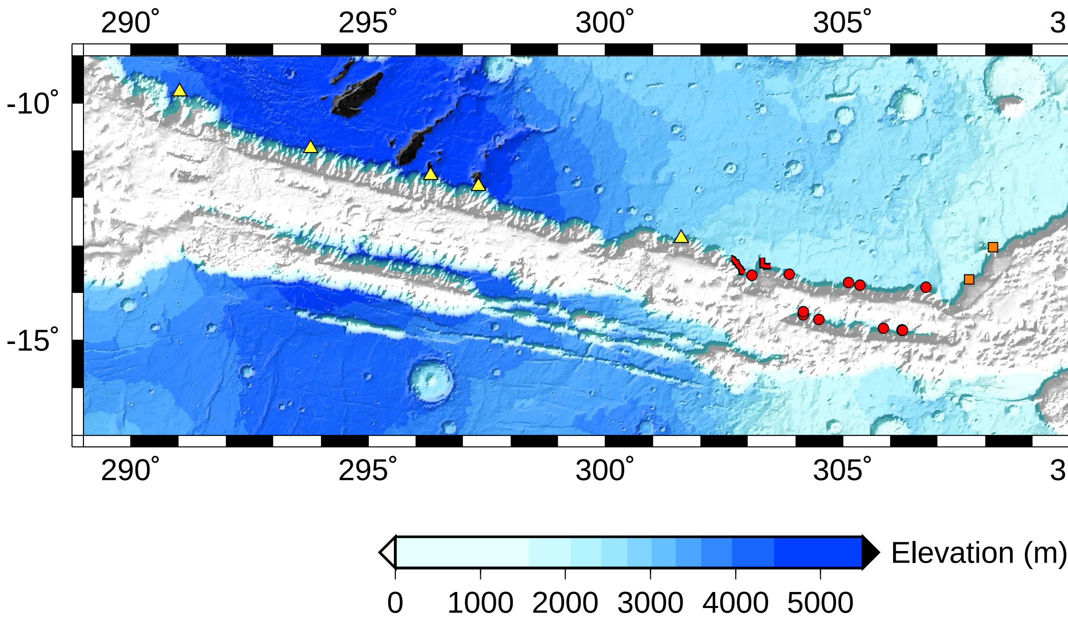

Figure 19: The 1/128th degree MOLA gridded data has been stretched to show a restricted elevation range to highlight the variability in the elevation of the plateau surface beyond the north rim of Coprates Chasma. Locations of topmost strong layer outcrops as seen in MOC images are noted by round red dots, and the two red lines indicate where the layer can be seen in THEMIS VIS images. The yellow triangles indicate those locations noted in Table 3 where a resistant layer is observed, but it is uncertain as to whether it is the same dark, competent layer noted by the circles. The orange squares indicate the locations of the approximately 70 m thick unit of resistant layers that cap the Capri Chasma edge.

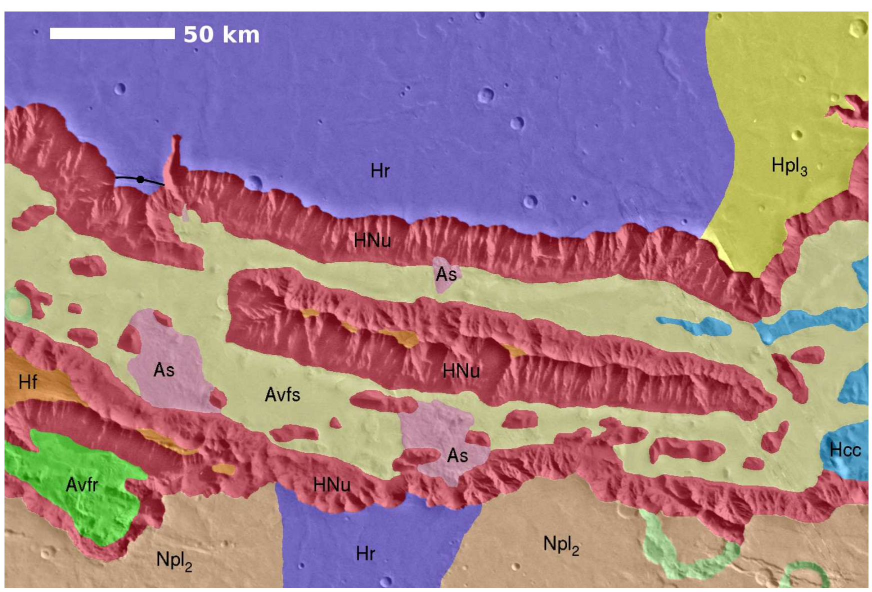

Figure 20: This unit map is simplified from the Witbeck et al. (1991) map, but uses the same notation, for more information see the original map. The following units are defined on that map: As - Slide material, Hcc - Chasma chaotic material, Avfs - Smooth floor material, Avfr - Rough floor material, Hpl_3 - Smooth unit, Npl_2 - Subdued cratered unit, Hf - Younger fractured material, Hr - Ridged plains, HNu - Undivided material. The black line and circle denote a fault that was identified by Witbeck et al. (1991) and is discussed in this study. Furthermore, the flat-topped areas along the top of the massif are marked as younger fractured material (Hf), but this study indicates that they are underlain by the same layered stack.

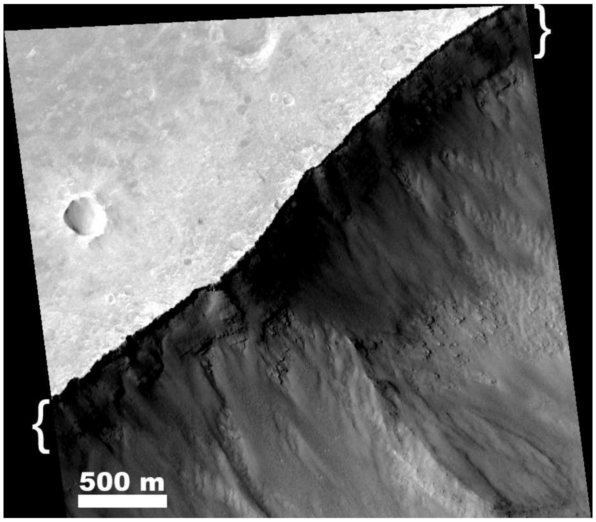

Figure 21: Portion of the MOC image E05/02164 showing that instead of a single thin strong layer, a stack of resistant layers underlies the the plateau here. Sequence is indicated with brackets.

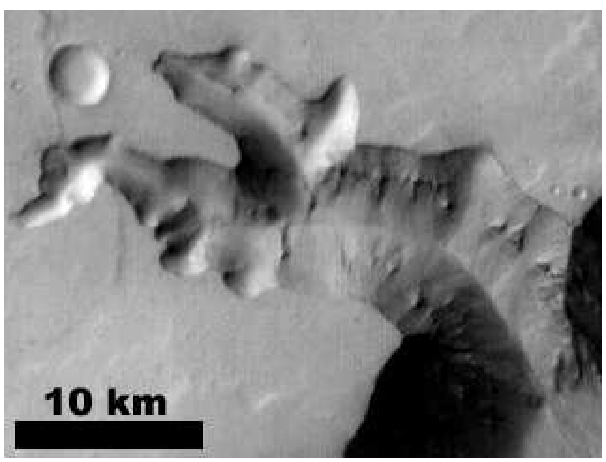

Figure 22: Portion of daytime THEMIS IR image I01875001, showing a small side chasma that cuts into the slope of Capri Chasma (Fig. 3) near 308° E, 13° S.

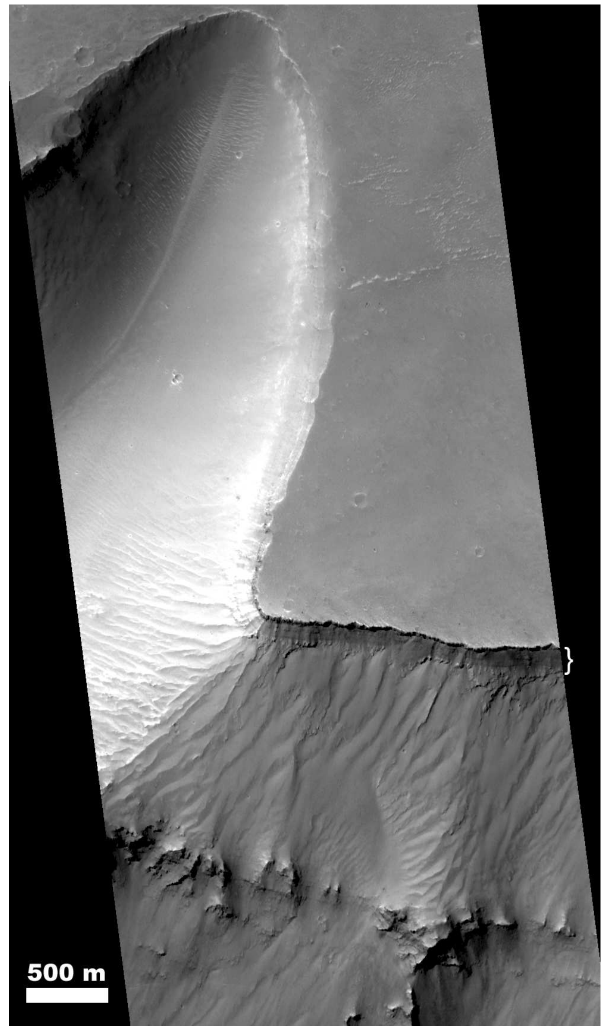

Figure 23: MOC image M02/03555 shows an east-west tributary chasma that opens from Capri Chasma and a shallow northward trending theater-headed depression. A cliff-forming sequence can be seen along the north rim of the tributary chasma (indicated with the bracket), but it becomes less discernible along the depression's east rim.

More evidence of a uniform stratigraphy beneath Aurorae Planum can be seen farther northeast along the Capri Chasma rim. E09/02363 and M08/05759 show a stack of resistant layers that form the chasma rim, then a massive unit, and another resistant unit from 800 to 500 m elevation. M07/01362 (Fig. 25) shows a strong cliff edge, and a possible dust cover on the plateau that appears to have receded back revealing a more rocky surface which appears to be the top of a layered stack 70 m thick, a massive section (possibly talus covered), and then resistant layering from 880 to 640 m elevation. Even farther northeast, M11/01959 also displays a distinct resistant layered stack, 70 m thick, that forms the chasma rim. This

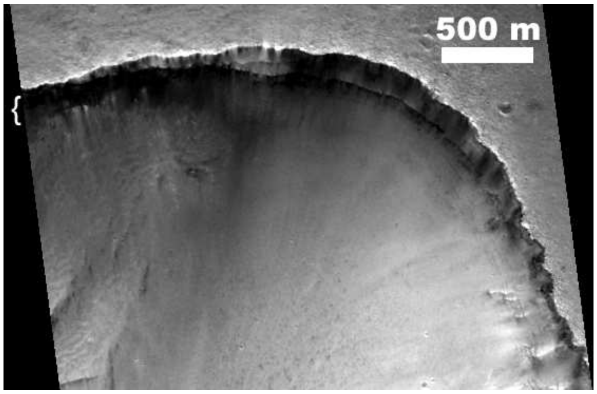

Figure 24: MOC image M09/04970 shows a side chasma from Capri Chasma (farther east from Fig. 23). A sequence of strong layers can be seen to outcrop below the plateau surface (indicated with the bracket). The sequence is more difficult to make out in this image than in Fig. 23 because the resolution is two times better in that image.

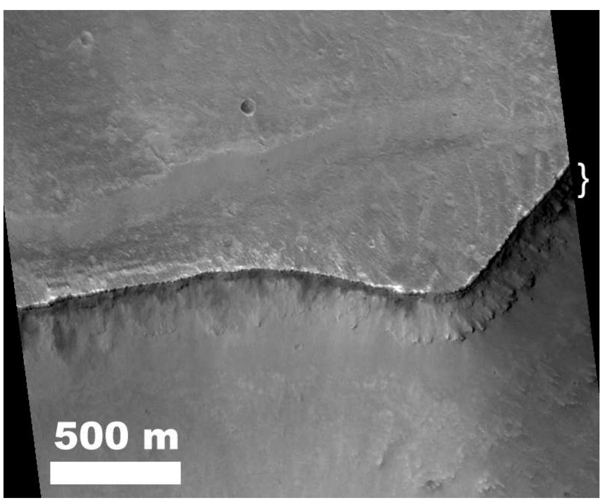

Figure 25: MOC image M07/01362 along the edge of Capri Chasma shows a resistant sequence of layered materials 70 m thick (indicated by the bracket) right up at the chasma rim, not covered by a mantle of other material.

image also shows a massive section (possibly talus covered) and then a resistant layered unit from 1040 to 840 m in elevation.

The expression of a $\geq$ 70 m thick unit of cliff-forming layers at the chasma rim followed below by a massive unit or talus covering, and then a resistant unit of 200 to 300 m thickness is observed along a 250 km stretch of Capri Chasma. These observations indicate a relatively consistent stratigraphy over a large distance and may also be indicative of the stratigraphy that underlies the entire Aurorae Planum. The elevation of the top of that 70 m thick unit varies by 200 m along that distance, but is still relatively flat-lying. Similarly, the outcrops of the resistant layer within the slope vary, but are also relatively flat-lying.

3.6 Thickness and extent of the topmost strong layer

We were unable to make a direct measurement with MOLA data of the thickness of the topmost layer in Coprates Chasma. However, based on elevation and slope information from the various outcrop locations and plan form extents in narrow angle MOC images, we estimate that its thickness is about 10 m.

Witbeck et al. (1991) interpreted both the the flat-topped areas along the spine of the massif and the plateau at the north rim as early Hesperian lava flows but mapped them differently based on their structural modification (normal faults on the massif, wrinkle ridges on the plateau, Fig. 20). Our observations indicate that both terrains are underlain by the same sequence of layers.

Our MOC and THEMIS VIS surveys of Coprates Chasma indicate that the topmost competent dark layer seen in the massif is also positively identified in the rim of Coprates Chasma directly north of the massif (Fig. 19). If we draw a simple polygon connecting these outcrops, we estimate a 8700 km^2 areal extent. This estimate does not take into account the unknown amount of north-south extension between the north slope and the massif. If we assume 60° fault surfaces, and that the floor of Coprates Chasma between the massif and the north wall was the former plateau surface, we can estimate that extension at about 7 km (the estimate rises to 8 km if the graben block is buried by a kilometer of fill). If we take this estimate of extension into account, then the area is only about 7000 km^2. However, both of these estimates assume that the layer terminates just inside the north wall, and doesn't account for how extensive the layer might have been before creation of the chasma. Due to this uncertainty, the true areal extent of this layer is likely to be greater than these values.

4 Discussion

We hypothesize that the stratigraphy exposed along the north rim of this section of eastern Coprates Chasma, along the edges of the massif, and along the rim of Capri Chasma are all a part of the same extensive stratigraphic stack present in this region. At many locations we observe a single, approximately 10 m thick, dark-toned, competent layer that appears to act as a resistant cap just below the break in slope between plateau surfaces and chasma slopes (Table 1, Fig. 19). Below that layer, there are a few hundred meters of lighter-toned, finely layered material that appears less competent. Below that we see a sequence of darker-toned competent layers, about ~ 100 m thick. Since this pattern is seen along the north rim of eastern Coprates Chasma, along the edge of the flat-topped areas of the massif, and to a lesser extent along the rim of Capri Chasma, we think that we are observing different portions of an extensive set of layers.

Using Viking Orbiter data, Treiman et al. (1995) identified a layering packet 400 m thick that they thought was ubiquitous throughout Valles Marineris. It was present at the chasmata rims with a similar thickness regardless of plateau elevation. From this data, they interpreted the layering to be the result of diagenetic processes. Although our study does not include all of the chasmata rims examined by Treiman et al. (1995), we can comment on those in eastern Coprates and Capri Chasmata. The topmost strong layer that we observe directly contradicts many of the arguments that study makes for diagenesis. We find that where the layer intersects a large crater, it is modified by the impact (Section 3.2 and Fig. 13), indicating that it was present prior to that impact. We find this layer to be at different depths below the plateau surface in different places. We do not find evidence of the topmost strong layer along the Capri Chasma rim, indicating the extent of this particular layer, furthermore we find differences between the north and south rims of eastern Coprates Chasma. Therefore, we find no evidence for the structural and stratigraphic "transgressions" indicated by Treiman et al. (1995), nor do we think that a diagenetic origin is likely for the layers observed along the rims of these chasmata.

Given the dark tone and relatively high strength of the few competent layers or competent layered units, we think that their most likely composition is that of a relatively dense basalt. The topmost competent layer exhibits a morphology and extent that is comparable to terrestrial flood basalts and inflated sheet flows (e.g. Keszthelyi and Self, 1998; Thordarson and Self, 1998; Keszthelyi et al., 2000). The presence of flood lavas on Mars has been suspected for some time (e.g. Greeley and Spudis, 1981; Mouginis-Mark et al., 1992; McEwen et al., 1999; Keszthelyi et al., 2000), and suggested recently by Ori and Karna (2003). The other competent layers farther down the stack are more difficult to characterize, and may be sequences of thin flows interbedded with tephra or other sediments. A basaltic composition for Valles Marineris in general is indicated by Phobos ISM (Murchie et al., 2000), TES (Bandfield et al., 2000), and THEMIS (Christensen et al., 2003a) measurements although specific layers are not resolved. Given the footprint sizes of these instruments (22 km/pixel for Phobos ISM, 3×9 km pixels for TES, and 100 m/pixel for THEMIS), they are probably sampling the intervening weak layers and talus to a large extent, although the strong layers could have stronger absorption bands, dominating the signal. The relatively weak layers (either volcanic tephra or sediments derived from competent volcanic material) are probably not thick competent lava flows, but could have a basaltic composition. It is expected that there is a much greater ratio of tephra to lava on Mars than on Earth (Wilson and Head, 1994). However, given the overall strength of the slopes (Schultz, 2002), the intervening relatively weak sequences are probably lithified, but not as strong as the thin dark-toned sequences.

4.1 Tectonic implications

In order to interpret our measurements of the topmost strong layer, we must make some assumptions about its original position. The topmost strong layer was either emplaced horizontally and subsequently altered by tectonic forces into the exposures that we measure today, or it was emplaced over an undulatory pre-existing surface, and the elevations where we observe it are the original locations of these outcrops, or a combination of these two. Based on the data that are available to us, we cannot truly determine which of these scenarios occurred, but there is some evidence that leads us to think that the layer was emplaced horizontally (for the most part), and the offsets observed within the massif are due to tectonic activity.

The apparent dips measured between the outcrops within the massif and the north rim are all quite low (Table 2), the largest being 3.65° dipping down to the south within the massif. Keszthelyi and Self (1998) indicate that long lava flows on the Earth can occur on slopes up to about 5°, and that the effect of reduced gravity would allow long lava flows on steeper slopes. So these slopes on their own, do not suggest tectonic movement.

In most locations where the next most competent sequence is observed, it has a consistent elevation difference with the topmost strong layer. Again, this by itself might only argue that the next most competent sequence was laid down on an undulatory surface, making its surface undulatory, and the overlying strata (topmost strong layer included) simply conformed to this surface.

However, all of these data together, combined with the observations of the down-dropped block (Section 3.1 and Fig. 9) and the down-dropped promontory surface(Section 3.4 and Fig. 17) lead us to the conclusion that the topmost strong layer was emplaced mostly horizontally. Therefore, the variety of elevations at which the topmost strong layer is observed are the result of tectonic movements, not just original emplacement at a variety of elevations. Additionally, this supports the theory that eastern Coprates Chasma underwent some north-south extensional motion and subsidence (Schultz, 1991, 1997, 1998; Lucchitta et al., 1992; Peulvast et al., 2001; Fueten et al., 2005) and the massif here is a horst block.

In addition to this large scale horst and graben structure, this portion of Coprates Chasma displays a kind of blunt-canyon morphology in the rim to the northwest of the massif, and there is a short north-south oriented re-entrant cut into the slope there (Fig. 16). That might be the remnant of a cross-fault (Wilkins and Schultz, 2003) that demarcated the western extent of the massif block.

The massif block subsided on the order of a hundred meters (over 350 m at the west end and 150 m at the east end), and it must have tilted down slightly to the west either during chasma formation or in the time since. We find two different measures of the north-south apparent dip of the topmost strong layer in the massif, so there must also be faults within the massif that are responsible for the apparent dip angle difference and allowed for a twisting motion within the massif. Additionally, the promontory to the west indicates subsidence on the south side of the graben identified there by Witbeck et al. (1991) of about 150 m.

While the apparent dip angles in the massif layer display a greater east-west tilt than the relatively flat-lying layer in the north slope, the measurements of the topmost layer outcrops there display a faint apparent dip down towards the west (Table 2). These measurements are consistent with the gradient of 0.03° found by Smith et al. (1999b) in the floor of Coprates Chasma east of about 300° E longitude. This similarity indicates that the gradient of the chasma floor may not be independent of the chasma slope rock strata in this region.

A qualitative observation can be made that the rim of Coprates Chasma directly north of the massif has a mostly linear trend, however farther westwards, the northern slope of Coprates Chasma contains more arcuate landslide alcoves, as do portions of the slope south of the massif. We hypothesize that the infrequent strong layers are contributing to both of these morphologic characters. These sequences of more resistant rock may be acting to provide structural support, and therefore their presence or absence is an important factor in the overall morphology of the slope. Thickness of individual resistant sequences, vertical density of such sequences, and even fault patterns within those sequences may be governing whether a particular stretch of chasma rim has a mostly linear trend with small spur-and-gully morphology or whether the rim is susceptible to large landslides. As slopes are eroded, the presence of resistant layers will provide structure and may help to maintain broad linear trends. However, these layers will also cause locally steepened slopes below them, eventually making these areas more susceptible to catastrophic failure, perhaps triggered by a seismic event (Schultz, 2002).

4.2 Boulders and blocks

Malin and Edgett (2001) note that there are few boulders observed at the bases of the slopes within Valles Marineris. They infer that particles derived from wall materials do not have sufficient strength to maintain large sizes during their descent to the base of the slope. Malin and Edgett (2000) indicate that where steep scarps occur in obviously volcanic terrain, boulders are often seen downslope.

In order to gain an understanding of the competency and strength of eroding units, we surveyed all MOC images with resolutions better than 4 m/pixel (up to 1.41 m/pixel) in the eastern Coprates Chasma

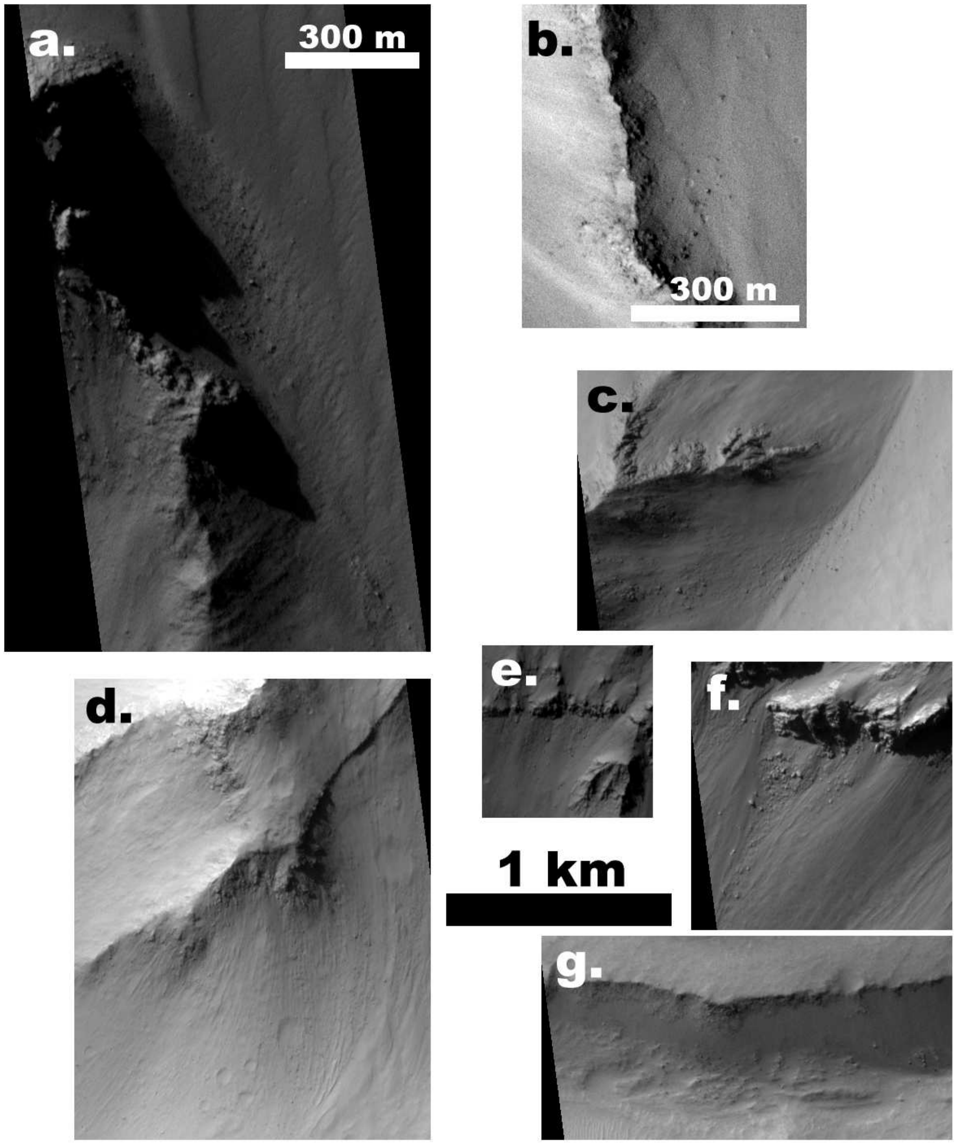

Figure 26: MOC images showing boulders and blocks on the slopes of Coprates Chasma. (a) Portion of MOC image M00/02438. (b) Portion of MOC image M07/00865. (c-e) Portions of MOC image E01/02131. (f) Portion of MOC image M21/01517. (g) Portion of MOC image M00/02870. Figures c through g share the same 1 km scale bar.

region to look for boulders and blocks. Objects must be at least two pixels in diameter to be observed under the best conditions. Objects would have to be many more pixels in diameter if the photometric conditions were less than perfect, or if the objects were largely buried. Given these size parameters we are looking for objects that fall into the very coarse boulder to coarse block categories of Blair and McPherson (1999). We will refer to all of the objects in this size range as blocks for simplicity.

We observed blocks in some images, at a host of different elevations on the slopes, but none on the flat floor of Coprates Chasma or near the base of the slopes. In all cases where we did observe blocks, it was clear that these blocks had been shed from strong layers immediately upslope of their locations (Fig. 26). We conclude that the strong layers here produce blocks of similar sizes as seen elsewhere on Mars, but that they either do not roll farther than about 1 km or do not survive transport over more than about 1 km.

Perhaps as the strong layers within the slope are broken up by the landslide process, the resultant particles either ride the surface of the landslide or are displaced upward from within. Either way, the blocks would suffer less damage than they would otherwise experience if they were to roll and fall down the entire slope (as suggested by Malin and Edgett, 2001). This scenario would explain why boulders and blocks are seen on landslide deposits on the Valles Marineris floor (Malin and Edgett, 2001), but not on the floor materials in general.

4.3 Wrinkle ridges and extent of the topmost strong layer

Wrinkle ridges are observed on Ophir Planum (Watters, 1991, 1993; Zuber and Aist, 1990; Mueller and Golombek, 2004). The recent quantitative model by Schultz (2000) indicates that wrinkle ridges are formed when a blind thrust fault occurs below layers which are capable of bedding plane slip, have large strength contrasts, or both. This stratigraphic situation is exactly what we observe along the north rim of Coprates Chasma. In fact, the topmost competent layer is only observed where the ridged plains unit is cut by slopes (Figures 19 and 20). If blind thrust faults occur at depth below the planum surface, then bedding plane slip might occur between the layers of different strength that we observe in the stratigraphic stack here. This slip could result in those layers forming a wrinkle ridge in the plateau surface material, as is observed across Ophir Planum. The observation of wrinkle ridges on Ophir Planum may be an indication that there is a uniformity of strata that underlies Ophir Planum, and more specifically we hypothesize that the topmost strong layer may underlie Ophir Planum.

Since wrinkle ridges and the ridged plains unit extend westwards on Ophir Planum from eastern Coprates Chasma, this may strengthen the interpretation that competent layers observed farther west (Fig. 19) are part of the same stratigraphic stack that we observe near the massif. However, whether it underlies the smooth unit (Hpl_3) and the younger fractured material (Hf) (Witbeck et al., 1991) of Ophir Planum west of 298° E is unknown. Schultz (1991) suggests that the ridged plains may underlie this area, with the wrinkle ridges buried beneath several hundred meters of material, but it is clear that he thinks it unlikely. It is possible that the same unit underlies both terrains, and that different tectonic forces, or different stratigraphies at depth are affecting its surface expression in different ways.

If the topmost strong layer is an extensive and continuous lava flow, there are only two ways for it to achieve the anticlinal shape indicated by the MOLA data (Fig. 19). One way is for the source vent for this sheet to be somewhere on the local elevation maxima, in which case this last volcanic flow would have occurred after the broad topography formed. Alternately, this sheet could have been emplaced mostly horizontally prior to crustal flexure in this area (Banerdt et al., 1992; Schultz and Tanaka, 1994; Mège and Masson, 1996), and then folded into an anticline. However this theory is speculative, as we cannot determine if the resistant layer observed in western Coprates Chasma along the north rim is the same topmost strong layer observed near the massif in the east. A greater amount of high-resolution coverage would be required along the chasma rim to make this correlation.

4.4 Depositional implications

Coupling our conservative areal estimate of the topmost strong layer (7000 km^2) with our estimated 10 m thickness yields a 70 km^3 volume estimate. If the material is a single lava flow, then this minimum volume of lava is similar to the smaller volume flood lava flow fields within the Columbia River Basalts on Earth (e.g. Tolan et al., 1989; Reidel et al., 1989; Keszthelyi and Self, 1998). For example, the Roza flow is 1300 km^3 (Keszthelyi and Self, 1998). Our thickness estimate for this Martian flow is also within terrestrial norms. Reidel et al. (1989) indicate that flows range in thickness from a few meters to about one hundred meters, averaging 30 m. These values are also within the range of lava flows measured on Mars (Table 4).

If we assume that this topmost strong layer underlies a sizable portion of the Witbeck et al. (1991) ridged plains (Hr) unit in Ophir Planum, then the volume estimate rises to over 2100 km^3. Although it is a large volume, it is still near the largest volume for a single terrestrial flood lava flow (Tolan et al.,

Lava Flow Characteristics Comparison

Source of Measurement	Location	Volume (km^3)	Thickness (m)
This study	Ophir Planum	70 - 2100	10
Cattermole (1990)	Alba Patera	0.6 - 5484	14 - 125
Lopes and Kilburn (1990)	Alba Patera	1.6 - 2310	28 - 75
Mouginis-Mark and Tatsumura Yoshioka (1998)	Elysium Planitia	17.7 - 68.1	40 - 60
Lanagan and McEwen (2005)	Cerberus plains	1800	20 - 40

Table 4: Comparison of example individual lava flows on Mars. The range of volumes on Alba Patera are from the differences between flows in the caldera and those on the flank. The range of volumes from Mouginis-Mark and Tatsumura Yoshioka (1998) are typical of their measurements, but the largest volume they estimated was 246 km^3.

1989; Reidel et al., 1989; Keszthelyi and Self, 1998), and still within reasonable values for measured martian flows.

The hypothesis that the topmost strong layer underlies, and is in fact partially responsible for the ridged plains of Ophir Planum has implications for the boundary between Ophir Planum and Aurorae Planum. As mentioned above, a morphological change across this boundary exists as noted by Witbeck et al. (1991), and the two plana have a subtle elevation difference of a few hundred meters from Ophir to Aurorae. Finally, the topmost strong layer is not observed at the Capri Chasma rim. We hypothesize that the boundary between Ophir and Aurorae Plana is the easternmost extent of the volcanic layer that we have been identifying as the topmost strong layer which crops out in Coprates Chasma.

The stack of resistant layers that marks the Capri Chasma rim may be the next sequence of resistant layers that is observed stratigraphically below the topmost strong layer in eastern Coprates Chasma in both massif and north rim outcrops (e.g. Fig. 27). The difference in elevation between Ophir Planum and Aurorae Planum could be because the topmost strong layer is not present, and the less resistant material observed between the topmost layer and the next resistant sequence has been eroded away (or was never there), such that the top of that resistant sequence forms the basement for the Aurorae Planum surface. This would indicate that Aurorae Planum must be older than Ophir Planum, although both are Hesperian in age. This age difference is supported by crater-count data in Table 1 of Witbeck et al. (1991). As observed along both Coprates and Capri Chasmata most outcrops of the topmost resistant layer show a mantle up to 100 m thick. This mantling material covers the surfaces of both Ophir and Aurorae Plana, smoothing the surficial transition between the two.

Depending on the timing of wrinkle ridge formation, the topographic break between Ophir and Aurorae may be a degraded wrinkle ridge. Subtle channels appear to dissect both plana, and may account for the theater headed depression incised on Capri Chasma. Potentially, the wrinkle ridge may have been present and blocked the topmost Coprates flow from entering Aurorae.

If we assume that the at least 70 m thick unit at the Capri Chasma rim underlies the Witbeck et al. (1991) smooth material unit (Hpl_3, Fig. 20) of Aurorae Planum, its volume would be at least 4000 km^3, more than that if it also underlies some portion of Ophir Planum. However, this unit is not a single lava flow, but many individual flows (we estimate each at tens of meters thick) layered on top of one another.

The south rim of Coprates Chasma shows no evidence for the topmost strong layer seen on the north rim and in the massif. Its absence may be partially responsible for the varying elevation of the south rim in this area. Erosional processes could act on the less resistant materials exposed here that are capped to the north by the topmost strong layer. The massif retains its flat-topped plateau remnants because that topmost strong layer and to a lesser extent the next resistant unit below it have been capping the massif against erosion, and strengthening it against mass wasting.

Additionally, the next most competent unit seen in the massif and the north rim are not identified here (possibly because its morphologic indicators are buried by talus). Geologic mapping suggests that older material is exposed at the surface south of Coprates Chasma, except some Hr east of the Coprates

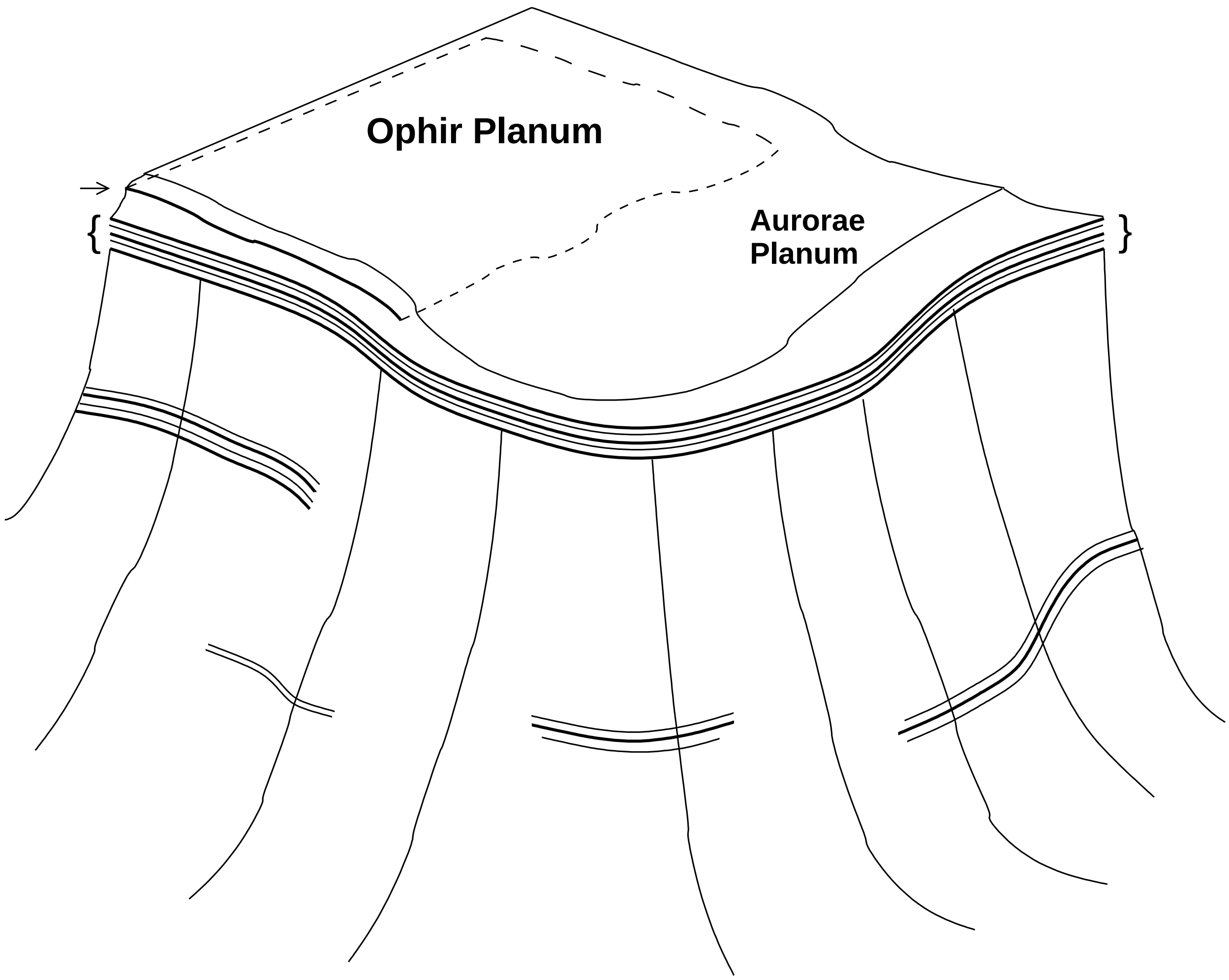

Figure 27: This sketch is a perspective view looking northwest at the boundary between Ophir and Aurorae Plana. To the left is Coprates Chasma and to the right Capri Chasma. It illustrates the hypothesis that the boundary between Ophir and Aurorae Plana is due to the eastern limit of the topmost strong layer (indicated by arrow, dashed lines give outline of buried strong layer). It also illustrates the hypothesis that the next most resistant layers (indicated by the brackets) observed below the topmost strong layer along the rim of Coprates Chasma is the same as the resistant sequence that forms the rim in Capri Chasma. The strong layers displayed below that are schematic.

rise. The area was probably active during the early Hesperian (Schultz and Tanaka, 1994). We think that these sequences are not present in the south rim simply because they did not get that far south during emplacement. There are many possible reasons for this, one possible hypothesis is that it was due to differential timing in the opening of the chasma. Perhaps the trough between what is now the massif and the south rim opened, then the strong layer was emplaced over the area of the plateau north of this proto-chasma, and then later the trough that separated the massif and the north rim opened.

The concept of a kilometers deep megaregolith a few kilometers below the surface (e.g. Carr, 1979, pp. 3000-3001; Tanaka and Golombek, 1989, p. 386; Davis and Golombek, 1990, pp. 14,244-

14,245; Clifford, 1993, p. 10,975) no longer seems viable (McEwen et al., 1999) in this area, where high rates of volcanism may have occurred during the Noachian and early Hesperian. The megaregolith may be present where early and middle Noachian surfaces were being heavily bombarded and gardened and not buried by ongoing volcanism. The topmost strong layer observed in Coprates Chasma, and the resistant sequence that forms the Capri Chasma rim show that indurated, bedded units are just below the plateau surfaces. These resistant layers are topped by a variable thickness of mantling material (less than 100 m). There are a few images where there may be a hint of bedding in this material, but it mostly appears fine-grained and massive at MOC resolution.

The individual strong layer that we see near the top of the layered stack of materials in this portion of Coprates Chasma is the exception, not the norm. We do not observe another individual layer by itself of this thickness, competency, or extent farther down-section in the strata where it crops out, although such individual layers would be readily covered by talus. More resistant bedded sequences are observed farther down-section that have a darker tone than surrounding units, and also form more resistant knobs and spurs. In locations not obscured by talus and mantling between these resistant units we observe lighter-toned, finely bedded units which are not as resistant to erosion. It is this material which appears to make up the largest part of the stratigraphic stack.

This dichotomy of strength in the slope materials is evident in the distribution of blocks within eastern Coprates Chasma. There is certainly an observational bias based on where there are images with resolutions better than 4 m/pixel, but blocks are only observed downslope of resistant layers. If entire slopes were composed primarily of resistant volcanic layers, we might expect a larger amount of observed blocks. Similarly, if the materials that formed the slopes were devoid of cliff-forming material, then no blocks should be seen. The fact that they are observed downslope of dark-toned, layered outcrops, indicates that these units are indeed relatively strong, but also infrequent in the stratigraphic stack. Lava breaks into blocks about the thickness of the lava unit, or the size of columnar joints within that unit (Milazzo et al., 2003). Blocks are not seen everywhere a resistant layer crops out perhaps because they are buried by talus, or roll down the slope so far that they are broken into smaller fragments. This lack of blocks is not surprising because it is rare on the Earth for such large blocks to be transported far without disruption.

5 Conclusions

Our observations indicate that the stratigraphy of Coprates Chasma consists of alternating thin (tens of meters) sequences of strong layers and thicker (hundreds of meters) sequences of relatively weak layers. The presence and extent of the infrequent strong layers which maintain steeper slopes have a large impact on chasma and slope morphology and that of the surrounding plana. Different combinations of strong and weak layers may have some impact into the varying morphologic character of chasmata within the Valles Marineris, as well as the locations and sizes of landslides. This difference in strength properties could also explain the paucity of observed boulders and blocks on Valles Marineris slopes if the thin strong layers are the only source of boulder-sized and larger particles.

Our ability to confidently trace layers decreases with decreasing elevation and slope. Layers near the top of the stack are easy to identify because they are not covered by talus. Similarly, mantling deposits can easily cloak outcrops of a strong unit on a relatively smooth slope, whereas just around a spur that same unit can be easily identified as a cliff former.

Understanding the stratigraphy has also led us to identify a strong layer near the top of the stratigraphic stack both in the north slope of eastern Coprates Chasma, and near the crest of the massif there. This massif is notable because it is one of the rare free-standing massifs within the Valles Marineris to retain its original flat-topped plateau surface. The massif preserves this surface because the strong layers are helping the massif resist erosion and collapse.

The elevation offset between the outcrops of this layer in the northern chasma slope and its outcrops in the massif indicate subsidence of the massif, most likely due to extensional fault motion. There are several models for how the Valles Marineris formed, including different combinations of rifting, collapse, and mass wasting. These observations confirm that extensional faulting was a contributing factor in the formation of this portion of Coprates Chasma.

It is still difficult to determine the origin of the less competent layers that make up the majority of the stratigraphic sequence of the Valles Marineris. Whether these layers in the Valles Marineris are fluvial, aeolian, or volcanic sedimentary layers, thin lava layers, welded tuff layers, or some combination of these, their contrast to the occasional strong units indicates a change in either the volcanic source or environmental conditions when these layers were emplaced.

The observations of the topmost strong layer in eastern Coprates Chasma indicate that the last basaltic lava flow in this area covered at least 7000 km^2, and possibly an increased area that consists of a large portion of Ophir Planum, either prior to or during chasma formation. The boundary between Ophir and Aurorae Plana may be the easternmost extent of this layer. Similarly, outcrops along Capri Chasma indicate that the Aurorae Planum surface is underlain by a stack of resistant layers that is also present stratigraphically below the strong layer which outcrops in eastern Coprates Chasma. These resistant layers are buried by 100 m or less of mantling material, which obscures the transition between the plana.

Acknowledgments

The authors would like to thank our colleagues H. J. Melosh, V. R. Baker, R. G. Strom, E. P. Turtle, and R. M. E. Mastrapa for their comments and criticisms of this work. The authors would also like to thank the reviewers, K. L. Tanaka and B. K. Lucchitta, for their valuable comments and suggestions. This research has made use of NASA's Astrophysics Data System. This research has made use of the USGS Integrated Software for Imagers and Spectometers (ISIS). It has also benefitted from the Generic Mapping Tools Software (Wessel and Smith, 1991, 1998), and color scheme guidance from Light and Bartlein (2004).

A Data

All data used in this paper came from NASA's Planetary Data System, and consists of the most recently released MOC (Malin and Caplinger, 1999, 2000) and THEMIS (Christensen et al., 2003b) data. The MOLA PEDR data used for elevation analysis in this paper is from version L, released on May 27, 2003 (Smith et al., 1999a).

B Differences from the Version Published by Elsevier

As noted on the first page, this paper was originally published by Elsevier, Inc. The differences between the paper published by Elsevier, Inc. and this document are essentially those of formatting. The text, figures and tables are identical, and this appendix has been added.

I have self-archived this paper by placing it on my own personal web site (under the terms outlined by Elsevier Inc.) as an excerise of one of the rights granted to me as an author of the work from Elsevier Inc. under our Licence Agreement.

To learn more about self-archiving and open access, visit the Self-Archiving FAQ at `http://www.eprints.org/self-faq/` and the Budapest Open Access Initiative at `http://www.soros.org/openaccess/`.

References

Archinal, B. A., Kirk, R. L., Duxbury, T. C., Lee, E. M., Sucharski, R., Cook, D., Mar. 2003. Mars Digital Image Model 2.1 Control Network. In: Lunar and Planetary Science XXXIV. No. #1485. Lunar and Planetary Institute, Houston (CD-ROM).

Bandfield, J. L., Hamilton, V. E., Christensen, P. R., Mar. 2000. A Global View of Martian Surface Compositions from MGS-TES. Science 287 (5458), 1626–1630.

Banerdt, W. B., Golombek, M. P., Tanaka, K. L., 1992. Stress and tectonics on Mars. In: Kieffer, H. H., Jakosky, B. M., Snyder, C. W., Matthews, M. S. (Eds.), Mars. The University of Arizona Press, Tucson, Ch. 8, pp. 249–297.

Blair, T. C., McPherson, J. G., Jan. 1999. Grain-Size and Textural Classification of Coarse Sedimentary Particles. Journal of Sedimentary Research 69 (1), 6–19.

Carr, M. H., Jun. 1979. Formation of Martian flood features by release of water from confined aquifers. Journal of Geophysical Research 84, 2995–3007.

Cattermole, P., Feb. 1990. Volcanic flow development at Alba Patera, Mars. Icarus 83, 453–493.

Christensen, P. R., Bandfield, J. L., Bell, J. F., Hamilton, V. E., Ivanov, A., Jakosky, B. M., Kieffer, H. H., Lane, M. D., Malin, M. C., McConnochie, T., McEwen, A. S., McSween, H. Y., Moersch, J. E., Nealson, K. H., Rice, J. W., Richardson, M. I., Ruff, S. W., Smith, M. D., Titus, T. N., Mar. 2003a. Early Results from the Odyssey THEMIS Investigation. In: Lunar and Planetary Science XXXIV. No. #1519. Lunar and Planetary Institute, Houston (CD-ROM).

Christensen, P. R., Gorelick, N., Mehall, G., Murray, K., Bender, K., Cherednik, L., 2003b. THEMIS Standard Data Archive. ODY-M-THM-3-IRRDR-V1.0 and ODY-M-THM-3-VISRDR-V1.0. NASA Planetary Data System.

Christensen, P. R., Jakosky, B. M., Kieffer, H. H., Malin, M. C., McSween, H. Y., Nealson, K., Mehall, G. L., Silverman, S. H., Ferry, S., Caplinger, M., Ravine, M., 2004. The Thermal Emission Imaging System (THEMIS) for the Mars 2001 Odyssey Mission. Space Science Reviews 110, 85–130.

Clifford, S. M., Jun. 1993. A model for the hydrologic and climatic behavior of water on Mars. Journal of Geophysical Research 98 (E6), 10973–11016.

Davis, P. A., Golombek, M. P., Aug. 1990. Discontinuities in the shallow Martian crust at Lunae, Syria, and Sinai Plana. Journal of Geophysical Research 95, 14231–14248.

Frey, H., Mar. 1979. Thaumasia - A fossilized early forming Tharsis uplift. Journal of Geophysical Research 84, 1009–1023.

Fueten, F., Stesky, R. M., MacKinnon, P., May 2005. Structural attitudes of large scale layering in Valles Marineris, Mars, calculated from Mars Orbiter Laser Altimeter data and Mars Orbiter Camera imagery. Icarus 175, 68–77.

Greeley, R., Spudis, P. D., Feb. 1981. Volcanism on Mars. Reviews of Geophysics and Space Physics 19, 13–41.

Keszthelyi, L., McEwen, A. S., Thordarson, T., Jun. 2000. Terrestrial analogs and thermal models for Martian flood lavas. Journal of Geophysical Research 105 (E6), 15027–15050.

Keszthelyi, L., Self, S., Nov. 1998. Some physical requirements for the emplacement of long basaltic lava flows. Journal of Geophysical Research 103 (B11), 27447–27464.

Kirk, R. L., Lee, E. M., 2005. MDIM 2.1: Mars Global Digital Image Mosaic.
URL `http://astrogeology.usgs.gov/Projects/MDIM21/`

Lanagan, P., McEwen, A. S., 2005. Geomorphic Analysis of the Cerberus Plains: Constraints on the Emplacement of the Youngest Lava Flows on Mars. Icarus in revision.

Light, A., Bartlein, P. J., Oct. 2004. The End of the Rainbow? Color Schemes for Improved Data Graphics. EOS Transactions 85, 385–391.
URL `http://geography.uoregon.edu/datagraphics/`

Lopes, R. M. C., Kilburn, C. R. J., Aug. 1990. Emplacement of lava flow fields - Application of terrestrial studies to Alba Patera, Mars. Journal of Geophysical Research 95, 14383–14397.

Lucchitta, B. K., Isbell, N. K., Howington-Kraus, A., Feb. 1994. Topography of Valles Marineris: Implications for erosional and structural history. Journal of Geophysical Research 99 (E2), 3783–3798.

Lucchitta, B. K., McEwen, A. S., Clow, G. D., Geissler, P. E., Singer, R. B., Schultz, R. A., Squyres, S. W., 1992. The canyon system on Mars. In: Kieffer, H. H., Jakosky, B. M., Snyder, C. W., Matthews, M. S. (Eds.), Mars. The University of Arizona Press, Tucson, Ch. 14, pp. 453–492.

Malin, M. C., Caplinger, M., 1999. MOC Decompressed Standard Data Product Archive. MGS-M-MOC-NA/WA-2-DSDP-L0-V1.0. NASA Planetary Data System.

Malin, M. C., Caplinger, M., 2000. MOC Standard Data Product Archive. MGS-M-MOC-NA/WA-2-SDP-L0-V1.0. NASA Planetary Data System.

Malin, M. C., Danielson, G. E., Ingersoll, A. P., Masursky, H., Veverka, J., Ravine, M. A., Soulanille, T. A., May 1992. Mars Observer Camera. Journal of Geophysical Research 97 (E5), 7699–7718.

Malin, M. C., Edgett, K. S., Dec. 2000. Sedimentary Rocks of Early Mars. Science 290, 1927–1937.

Malin, M. C., Edgett, K. S., Oct. 2001. Mars Global Surveyor Mars Orbiter Camera: Interplanetary cruise through primary mission. Journal of Geophysical Research 106 (E10), 23429–23570.

McEwen, A. S., Malin, M. C., Carr, M. H., Hartmann, W. K., Feb. 1999. Voluminous volcanism on early Mars revealed in Valles Marineris. Nature 397, 584–586.

Mège, D., Cook, A. C., Garel, E., Lagabrielle, Y., Cormier, M., May 2003. Volcanic rifting at Martian grabens. Journal of Geophysical Research 108 (E5), 10–1.

Mège, D., Masson, P., Dec. 1996. Stress models for Tharsis formation, Mars. Planetary and Space Science 44, 1471–1497.

Milazzo, M. P., Keszthelyi, L. P., McEwen, A. S., Jaeger, W., Mar. 2003. The Formation of Columnar Joints on Earth and Mars. In: Lunar and Planetary Science XXXIV. No. #2120. Lunar and Planetary Institute, Houston (CD-ROM).

Mouginis-Mark, P., Tatsumura Yoshioka, M., Aug. 1998. The long lava flows of Elysium Planita, Mars. Journal of Geophysical Research 103 (E8), 19389–19400.

Mouginis-Mark, P. J., Wilson, L., Zuber, M. T., 1992. The physical volcanology of Mars. In: Kieffer, H. H., Jakosky, B. M., Snyder, C. W., Matthews, M. S. (Eds.), Mars. The University of Arizona Press, Tucson, Ch. 13, pp. 424–452.

Mueller, K., Golombek, M., Jan. 2004. Compressional Structures on Mars. Annual Review of Earth and Planetary Sciences 32, 435–464.

Murchie, S., Kirkland, L., Erard, S., Mustard, J., Robinson, M., Oct. 2000. Near-Infrared Spectral Variations of Martian Surface Materials from ISM Imaging Spectrometer Data. Icarus 147 (2), 444–471.

Ori, G. G., Karna, A., Mar. 2003. The Uppermost Crust of Mars and Flood Basalts. In: Lunar and Planetary Science XXXIV. No. #1539. Lunar and Planetary Institute, Houston (CD-ROM).

Peulvast, J.-P., Mège, D., Chiciak, J., François, C., Masson, P. L., 2001. Morphology, Evolution and Tectonics of Valles Marineris Wallslopes (Mars). Geomorphology 37, 329–352.

Reidel, S. P., Tolan, T. L., Hooper, P. R., Beeson, M. H., Fecht, K. R., Bentley, R. D., Anderson, J. L., 1989. The Grande Ronde Basalt, Columbia River Basalt Group; stratigraphic descriptions and correlations in Washington, Oregon, and Idaho. In: Reidel, S. P., Hooper, P. R. (Eds.), Volcanism and Tectonism in the Columbia River Flood-Basalt Province. No. 239 in Special Papers (Geological Society of America). Geological Society of America, Inc., pp. 21–53.

Schultz, R. A., Dec. 1991. Structural development of Coprates Chasma and western Ophir Planum, Valles Marineris Rift, Mars. Journal of Geophysical Research 96, 22777–22792.

Schultz, R. A., Jun. 1997. Displacement-length scaling for terrestrial and Martian faults: Implications for Valles Marineris and shallow planetary grabens. Journal of Geophysical Research 102 (B6), 12009–12016.

Schultz, R. A., Jun. 1998. Multiple-process origin of Valles Marineris basins and troughs, Mars. Planetary and Space Science 46, 827–834.

Schultz, R. A., May 2000. Localization of bedding plane slip and backthrust faults above blind thrust faults: Keys to wrinkle ridge structure. Journal of Geophysical Research 105 (E5), 12035–12052.

Schultz, R. A., Oct. 2002. Stability of rock slopes in Valles Marineris, Mars. Geophysical Research Letters 29 (19), 38–1.

Schultz, R. A., Tanaka, K. L., Apr. 1994. Lithospheric-scale buckling and thrust structures on Mars: The Coprates rise and south Tharsis ridge belt. Journal of Geophysical Research 99 (E4), 8371–8385.

Sharp, R. P., 1973. Mars: Troughed Terrain. Journal of Geophysical Research 78, 4063–4072.

Smith, D. E., Neumann, G., Ford, P., Arvidson, R. E., Guinness, E. A., Slavney, S., 1999a. Mars Global Surveyor Laser Altimeter Precision Experiment Data Record. MGS-M-MOLA-3-PEDR-L1A-V1.0. NASA Planetary Data System.

Smith, D. E., Zuber, M. T., Frey, H. V., Garvin, J. B., Head, J. W., Muhleman, D. O., Pettengill, G. H., Phillips, R. J., Solomon, S. C., Zwally, H. J., Banerdt, W. B., Duxbury, T. C., Golombek,

M. P., Lemoine, F. G., Neumann, G. A., et al., Oct. 2001. Mars Orbiter Laser Altimeter: Experiment summary after the first year of global mapping of Mars. Journal of Geophysical Research 106 (E10), 23689–23722.

Smith, D. E., Zuber, M. T., Solomon, S. C., Phillips, R. J., Head, J. W., Garvin, J. B., Banerdt, W. B., Muhleman, D. O., Pettengill, G. H., Neumann, G. A., Lemoine, F. G., Abshire, J. B., Aharonson, O., Brown, D. C., Hauck, S. A., Ivanov, A. B., McGovern, P. J., Zwally, H. J., Duxbury, T. C., May 1999b. The Global Topography of Mars and Implications for Surface Evolution. Science 284 (5419), 1495.

Tanaka, K. L., Golombek, M. P., 1989. Martian tension fractures and the formation of grabens and collapse features at Valles Marineris. In: Lunar and Planetary Science Conference XIX. pp. 383–396.

Thordarson, T., Self, S., Nov. 1998. The Roza Member, Columbia River Basalt Group: A gigantic pahoehoe lava flow field formed by endogenous processes? Journal of Geophysical Research 103 (B11), 27411–27445.

Tolan, T. L., Reidel, S. P., Beeson, M. H., Anderson, J. L., Fecht, K. R., Swanson, D. A., 1989. Revisions to the estimates of the areal extent and volume of the Columbia River Basalt Group. In: Reidel, S. P., Hooper, P. R. (Eds.), Volcanism and Tectonism in the Columbia River Flood-Basalt Province. No. 239 in Special Papers (Geological Society of America). Geological Society of America, Inc., pp. 1–20.

Treiman, A. H., Fuks, K. H., Murchie, S., 1995. Diagenetic layers in the upper walls of Valles Marineris, Mars: Evidence for drastic climate change since the mid-Hesperian. Journal of Geophysical Research 100, 26339–26344.

Watters, T. R., Aug. 1991. Origin of periodically spaced wrinkle ridges on the Tharsis Plateau of Mars. Journal of Geophysical Research 96, 15599–15616.

Watters, T. R., Sep. 1993. Compressional tectonism on Mars. Journal of Geophysical Research 98 (E9), 17049–17060.

Wessel, P., Smith, W. H. F., 1991. Free software helps map and display data. EOS Trans. Amer. Geophys. U. 72 (41), 441, 445–446.

Wessel, P., Smith, W. H. F., 1998. New, improved version of Generic Mapping Tools released. EOS Trans. Amer. Geophys. U. 79 (47), 579.

Wilkins, S. J., Schultz, R. A., Jun. 2003. Cross faults in extensional settings: Stress triggering, displacement localization, and implications for the origin of blunt troughs at Valles Marineris, Mars. Journal of Geophysical Research 108 (E6), 10–1.

Williams, J., Paige, D. A., Manning, C. E., Jun. 2003. Layering in the wall rock of Valles Marineris: intrusive and extrusive magmatism. Geophysical Research Letters 30 (12), 25–1.

Wilson, L., Head, J. W., Aug. 1994. Mars: Review and analysis of volcanic eruption theory and relationships to observed landforms. Reviews of Geophysics 32, 221–263.

Witbeck, N. E., Tanaka, K. L., Scott, D. H., 1991. Geologic Map of the Valles Marineris Region, Mars. No. MAP I-2010. United States Geologic Survey.

Zuber, M. T., Aist, L. L., Aug. 1990. The shallow structure of the Martian lithosphere in the vicinity of the ridged plains. Journal of Geophysical Research 95, 14215–14230.

Zuber, M. T., Smith, D. E., Solomon, S. C., Muhleman, D. O., Head, J. W., Garvin, J. B., Abshire, J. B., Bufton, J. L., May 1992. The Mars Observer laser altimeter investigation. Journal of Geophysical Research 97 (E5), 7781–7797.